Universidade de Aveiro
2008
Departamento de Electrónica, Telecomunicações e Informática

Jacek Lukasz Kustra

Remoção de balistocardiograma em EEG-fMRI baseada numa abordagem de alinhamento temporal não linear

Universidade de Aveiro
2008
Departamento de Electrónica, Telecomunicações e Informática

Jacek Lukasz Kustra

Remoção de balistocardiograma em EEG-fMRI baseada numa abordagem de alinhamento temporal não linear

Dissertação apresentada à Universidade de Aveiro para cumprimento dos requisitos necessários à obtenção do grau de Mestre em Engenharia Biomédica, realizada sob a orientação científica do Dr. João Paulo Cunha, Professor Associado do Departamento de Electrónica, Telecomunicações e Informática da Universidade de Aveiro

If I have seen further,
it is by standing on the
shoulders of giants

Isaac Newton

À minha fantástica família...

o júri

presidente

Professor Doutor João Paulo Cunha
Professor Associado da Universidade de Aveiro

vogais

Professor Doutor Francisco António Cardoso Vaz
Professor Catedrático Aposentado da Universidade de Aveiro

Professor Doutor Miguel de Sá e Sousa de Castelo Branco
Professor Auxiliar da Universidade de Coimbra

Professor Doutor José Maria Amaral Fernandes
Professor Auxiliar convidado da Universidade de Aveiro

palavras-chave

Cérebro, imagiologia, electroencefalografia, ressonância magnética, artefacto, processamento de sinal

resumo

A análise multimodal do cérebro tem sido um importante tema de estudos recentes. A observação deste recorrendo a técnicas como a ressonância magnética funcional (RMF) permitem avanços significativos na análise, devido à sua resolução espacial, faltando no entanto a desejada revolução temporal. A observação simultânea recorrendo a RMF e outras técnicas como Electroencefalografia (EEG), devido à sua complementaridade na resolução espacial e temporal, tornam-se numa importante ferramenta para a comunidade médica. No entanto, devido aos fortes campos magnéticos encontrados dentro do scanner, a aquisição simultânea induz artefactos no EEG, ocultando o sinal fisiológico. Dois artefactos principais podem ser identificados: O artefacto de gradiente, devido aos campos magnéticos de alta frequência, e o Balistocardiograma, devido à actividade cardíaca do sujeito e ao forte campo magnético estático. Esta dissertação apresenta uma introdução à RMF, EEG e as vantagens da sua combinação, explorando as diferentes técnicas e limitações destas para a remoção dos artefactos. As técnicas mais frequentemente utilizadas para este fim, apesar da sua simplicidade, assumem sinais biomédicos como determinísticos, e desta forma nem sempre conseguindo remover o artefacto da forma mais eficiente. Um algoritmo capaz de se adaptar às variações naturais do artefacto é apresentado e a sua eficiência é estudada tanto em contexto de simulação como em sinais reais.

keywords

Brain, imaging, electroencephalography, magnetic resonance, artifact, signal procesing

abstract

Multimodal brain analysis has been the scope of many recent studies. Functional magnetic resonance imaging show remarkable advances in the study of the brain, because of its good spatial resolution, lacking however the desired time resolution. By simultaneously imaging the brain with gold standard techniques for the observation of the brain dynamics, such as Electroencephalography, the complementary advantages become a valuable tool for the medical community. Because of the strong static and varying magnetic fields found in the scanner, this simultaneous acquisition induces artifacts in the EEG, obscuring the underlying physiological signal. Two main artifacts can be identified: The Gradient artifact, caused by the fast changing magnetic fields and the Ballistocardiogram artifact, due to the cardiac activity and the strong static magnetic field. This dissertation presents an overview of both EEG and fMRI, showing the added value of combining them together, and explores different techniques of overcoming the induced artifacts. The most frequently used techniques, although simple, assure biomedical signals as deterministic and end up distorting the underlying physiological signal to a certain degree. An algorithm capable of adapting to the artifacts variations is presented and analyzed with simulated and real signals.

Contents

List of Figures

List of Tables

Chapter 1

Introduction

The beginning of knowledge is the discovery of something we do not understand.
Frank Herbert

The Brain is the central and most complex organ in the Human body. It is part of the central nervous system that is constituted by the brain and the spinal cord. All the sensory information is processed by this organ, and it is responsible for all the body control systems and intelligence that allow animals to see, feel, walk and perform decisions. As in most of mammal bodies, the brain is a symmetrical organ, with the left portion controlling the right side of the body and the right side controlling the left side. This is the result many of ages of evolution where this configuration provided the best possible protection, and minimizing the consequences of injuries on one side of the body. One of the most amazing achievements of the brain is allowing a being to have conscience of itself, questioning its own functioning.

The size of the brain greatly varies among species. One could think of its size as a measure of intelligence. However, since the brain is responsible for receiving all the sensory information, and sending information to the internal organs, it would be logical to consider that bigger bodies required larger brains. A more fair approach to this problem is to compare the relative size of the brain with the rest of the body. In this field, the Human species is among the species with the largest relative brain[42]. Although the brain is a highly optimized organ, composed of millions of different possible configurations, allowing us to perform very complex activities, like reading this thesis, the malfunction of the brain limits beings from performing a *normal* life. Brain pathologies can cause motor, sensory and intelligence limitations, so the quest to understand those pathologies and finding solutions to them has been a long started Human kind quest.

Before the discovery of the X ray application to medical imaging, the brain was only accessible by direct observation, which could reveal its shape, anatomy, both on cadavers and *in*

vivo. The study of it's function was very limited as only certain lesions, that limited the subject in some observable way, could suggest that brain area was responsible for that function. Technology has provided new ways to observe the human body by exploring different physical properties like the tissue radiation susceptibility (X ray, computer tomography), the electric potential difference through electroencephalography (EEG) or the nuclear spin (magnetic resonance imaging). Current techniques of brain function observation can be separated on direct and indirect methods. On direct methods, the brain is observed by directly measuring its activity. This can be achieved with EEG measured on the scalp surface, providing a direct measure of the underlying physiological effects. Indirect methods measure the consequences of brain activity, thus, indirectly measuring its activity. A principle used in this studies is that an increase in brain activity is closely related to an increase in blood flow in the active area. This property has been explored to in different methods like Positron Emission Tomography (PET) where the injection of a short-lived radioactive tracer isotope in the blood flow allows the observation of the active area. Functional Magnetic resonance imaging allows a fully non invasive method to explore this same principle, using the differences in blood oxygenation to achieve this goal.

1.1 The scope of this Thesis

The scope of this thesis is to present a method of brain function observation based on functional Magnetic Resonance Imaging (fMRI) and Electroencephalography (EEG). Both these techniques have proved their value, one in observing the brain electrical activity and the other in the indirect observation of the brain function by means of the hemodynamic response. However, their combination is not straightforward as the magnetic fields found inside the scanner induce artifacts in the EEG, obscuring the signal. In this thesis, we explore techniques for the removal of the induced artifacts and present a new approach for its removal.

The following two chapters (2 and 3) present an insight of the two observation techniques, covering the underlying physiological phenomenons that originate the observed signals. The physical principles used in the magnetic resonance imaging are briefly covered, illustrating the source of the artifacts found in the EEG acquired inside an MRI scanner. The EEG-fMRI chapter (4) analises the integration of the respective techniques. The state of the art of the artifact removal techniques are covered in depth showing the weaknesses and strengths of each. Finally on chapter 5, a new algorithm that intends to improve the weaknesses of the most commonly used approaches in artifact removal is presented. It's implementation details are covered and the results from using this algorithm are compared with the most commonly used methods.

1.2 Contributions

This thesis presents an overview of the most commonly used brain observation techniques (fMRI and EEG) showing the potential of the combination of both and the problems with this technique. The state of the art of the signal processing techniques is presented and its limitations are taken in account. A new algorithm for the EEG signal when acquired simultaneously with fMRI is presented and explored. A four page paper on this work has been submitted and accepted on the *14-th Nordic - Baltic Conference on Biomedical Engineering and Medical Physics, Riga, Latvia 16-20 June 2008.*

Chapter 2

Electroencephalography

If the presence of electricity can be made visible in any part of the circuit, I see no reason why intelligence may not be transmitted instantaneously by electricity.
Samuel Morse

Electroencephalography (EEG) is the neurophysiologic measurement of the electrical activity on the scalp surface. It is primarily used in the study of the properties of cerebral and neural networks in neuroscience [33]. The presence of electricity in animals has been a long known phenomenon. Back in 1790, Aldin used electric shocks in (failed) attempts to awaken the dead and one year after, Galvani discovers animal electricity. The first reports on brain electrical activity date back to 1833 when Ernest Fleish von Marxow describes electrical activity on the visual cortex. It wasn't't until 1873 that Caton first described the observation of *continuous spontaneous electrical activity* from the brain surface. Hans Berger pioneered in the studies of human EEG in 1920 and is usually credited for it's invention[45]. Since then, the EEG has become a gold standard tool for the observation of brain activity because of its non-invasive nature and very good temporal resolution. With modern digital approaches, it became possible to run various digital algorithms on the acquired signal allowing a better interpretation of the signals. Possible applications are the spike detection and artifact removal applications, which is further explored in this thesis.

2.1 The source of the electrical activity

In order to correctly interpret the measured electrical activity, we should understand its source. The EEG measures the potential difference across the scalp or directly on the cortex. This potential difference results from the underlying brain activity. This section briefly explores the physiological aspects that give rise to the measured potential differences. If we

observe the brain tissue under a microscope, the cortex appears as a network of fibers and nerves. While the neurons are located on the cortex surface, the white matter is found to be composed by fibers. These fibers connect the neurons to each other and allow a communication and information transmission between different brain areas. Both neurons and fibers are mainly composed of fluid contained within tubular membranes. In nerve fibers, the membrane is continuous along the whole length and can be covered with an insulating layer of myelin which terminates as the fiber ends the cell body. This membrane restricts the interchange of materials such as ions between the inside and the outside of the cells. This ionic restriction results in the establishment o a voltage, between the inside and the outside of a neuron or fiber, called the **resting potential**. In order to maintain this balance, energy is continually used to preserve it. Although this stead state can be disturbed, regulatory mechanisms exist that are *designed* to protect the fibers and cells. To transmit information from one place to another, a progressive transient disturbance of the resting potential is used. This is caused by a very rapid change of the membrane permeability to sodium ions followed by a quick recovery. This transmission phenomenon is called the **action potential** which consists of three stages:

Resting Stage At this stage, before the transmission begins, the membrane is said to be polarized. This implies a voltage difference of -90mV at the membrane.

Depolarization Stage Here, the membrane becomes permeable to sodium ions. The resting voltage of -90mV is immediately neutralized. In larger nerve fibers an overshot can occur and the membrane becomes positive. However, in most fibers, it rapidly approaches zero voltage and does not overshoot.

Re-polarization Stage Right after becoming permeable to sodium ions, the sodium channels start closing and potassium channels open causing a diffusion of potassium to the exterior. The membrane recovers it's negative potential.

Since an excited membrane portion usually excites the adjacent portions of the membrane, this results in a propagation in all directions away from the source. As the action potential propagation reaches the cell, it's permeability increases, causing it to generate a spike potential of it own. This response spreads through the dentritic branches and consequently transmitter substances are released.

The described activity generates electric potential differences on the cortex. The measured activity is the result from many simultaneous discharges rather than isolated spikes, since even the smallest electrodes are much larger than individual neurons. Also, the potential differences, when passing through the different physiological layers, are integrated, and its

potential is attenuated. The greatest attenuator and integrator in this process is the scull, so great advantages are found in measuring the electrical activity directly on the scalp. This procedure allows to find different patterns with very small electrode separation and also a larger signal amplitude. When measuring the potential differences on the scalp, much of this spatial precision is lost together with the signals amplitude, and although the temporal resolution is still very acceptable, the spatial resolution becomes very limited. However, the fact that the measurement on the scalp is a non invasive method, it usually greatly suppresses the advantages of measurement on the cortex.

2.2 Electrical Activity Patterns

When measuring the brain electrical activity, common patterns are found, that correspond to different states of brain activity and different levels of mental activity. Most of these are classified into one of the following five groups[41]:

Delta $<$ 4 Hz Usually found in children and during some sleep stages

Theta (5 - 8) Hz Associated with children and adolescents, can be also found during lucid dreaming and in the pre fall asleep period.

Alpha (8 - 12) Hz Alpha waves are associated with a waken but relaxed state. When the concentration focuses on something, this pattern disappears, being replaced by the higher frequency but lower amplitude Beta waves. This pattern often appears when the subjects eyes are closed since visual sensations cause its immediate cessation.

Beta $>$ 12 Hz This activity can be measured during active thinking and concentration.

Gama (26 - 100) Hz Associated to high mental activity and consciousness.

As referred, some of these patterns can be associated to different mental activity. With the proper training, an individual can learn to a certain degree to control some of these patterns. These EEG Feedback are becoming increasingly popular, and this principle has found many clinical applications[31]:

- Attention deficit / hyperactive disorder (ADHD)
- Depression
- Chronic Anxiety Disorder
- Chronic Alcoholism

- Epilepsy

Although there has been reported success in EEG feedback applications, there is still a long way to go as many problems arise, like differences found in the EEG patterns through age, which limit its practical widespread application.

2.3 Electrode Placement

Each electrode[1] is placed on the subjects scalp with the connected to one input of a differential amplifier, and the other input is connected to the selected reference. Depending on the chosen reference, different montages result:

Common Reference Deviation In this montage the potential difference for each electrode is measured against a selected electrode. The usual location of this electrode is on the scalp mid-line.

Average Reference Deviation All the inputs from the electrodes are averaged, and this value is used as common reference for each amplifier.

Bipolar Deviation This configuration implies that the amplifiers are connected in series. This way each amplifier measures the voltage difference between the current electrode and the next.

Each amplifier output is considered a *channel*. The channel positions are defined through standard scalp positions defined by the 10-20, 10-10 or 10-5 systems. Each number corresponds to the inter-electrode distance. In the original 10-20 standard, the positions are named after the first letter of the corresponding lobe, followed by a number representing its position. Odd numbers are used for the left side, whereas even numbers are used to specify the right side of the scalp[24].
The 10-20 system has stood as the mostly used standard, Although it's main purpose was to provide a reproducible method for placing a relatively small amount[2] of electrodes. With the modern development of multi-channel EEG amplifiers and 3d source localization techniques are applied whose precision increases with the number of electrodes, the need to place more electrodes took the standards one step further with the 10-10 system allowing an 81 channel density. However since high end users seeked even more precision, and 128 channel EEG

[1]The most commonly used electrodes are Ag/AgCl, which are placed on the subjects scalp through the use of a conducting Gel. Recent evolutions have been made with the development of a dry electrode technology, dispensing the use of the gel. [17]

[2]For today standards

became a common commercial choice, the 10-10 system was extended to the 10-5 system allowing the use of more than 300 electrode locations[25].

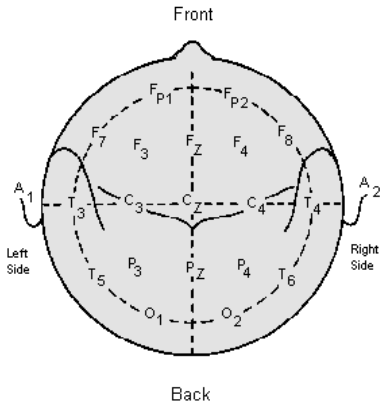

Figure 2.1: **10/20 Electrode placement**

The acquired signal is usually filtered with a high pass filter of 0.5Hz and a low pass ranging from 35-70Hz, depending on the signal quality and desired application. An additional notch filter is usually needed to remove the 50Hz/60Hz electric current frequency.

The resulting signals are used to sketch the signal. Classic Electroencephalographers connected these output to a mechanical system which represented the signal on a continuous roll of paper. Modern approaches use an Analog to Digital Converter (ADC) to sample each channel on the amplifier output. This allows the digital signal storage, offline analysis and opens the EEG signal to the Digital Signal Processing possibilities.

The measured signals can be analysed by a classical approach by directly analysing the sketched waves, or alternatively can be used in EEG inverse problem. The goal of this approach is to localize a finite element model of a patients head. By having a well defined electrode mesh, and taking some *a priori* assumptions about the anatomical conductivity, a source localization inverse problem is performed and by this means, the position and moment of the dipole are determined. This can lead to a better epileptic focus localization by using non invasive techniques[16].

2.4 The source localization Problem

The information about the activity source, or spatial localization, is very limited in EEG. Inverse Problem solution, aims in determining the source of the electric activity. These methods make some a priori assumptions that are sometimes hard to justify and prove. These can be divided in two categories: the dipole based, which assume a localized source

and distributed source methods, that assume many sources with different characteristics. The various brain activities can be separated by the use of Blind Source Separation (BSS) algorithms. This can further enhance the localization by separating distinct activity. There have been many advances in this field by the use of Intelligent Blind Signal Processing[3]. In order to separate mixed signals we need to make assumptions about in what way they are different, like statistical independence. In the case of neural activity, that is complicated to define this characteristics, artificial neural networks can be used to provide some "intelligence" to the demising process.

2.5 EEG artifacts

The EEG is intended to measure, as closely as possible the brains electrical activity. However, because of the small signal amplitude and high system sensitivity, the signal may become corrupted by many sorts of unwanted signals: the artifacts. The sources of these artifacts can be either generated by physiological sources, such as muscle movement, by external sources or even the combination of both.

The most common physiological artifacts found on an EEG are the ones caused by ocular (Figure 2.2) and tongue movements, muscle activity, the Electrocardiogram (ECG), pulse, respiration and skin properties[47].

Muscle activity The muscle activity is usually not periodic and can be easily identified on the EEG. However in cases of Parkinson disease, this artifact can become rhythmic, making it more difficult to separate it from the underlying brain activity.

Eye movement Eye movement artifacts can be identified on electrodes placed close to the subject eyes, and are useful in identifying different sleep stages. The Rapid Eye Movement (REM) stage, usually associated with dreaming can be clearly observed by the identification of the EEG eye movement associated artifacts.

Glossokinetic artifact In the same way as the previously explained artifacts, the tongue can be a source of artifact. Although it can be controlled by the patient, it can become a problem in uncooperative patients or the ones suffering from dementia.

Electrocardiogram Since the heart pulse is controlled by electrical impulses, these are also useful in diagnosing different heart conditions. The electrocardiogram (ECG), has its largest potential differences in the chest area. It interferes with the EEG signals, so physicians should also record the ECG so the artifacts can be temporally identified.

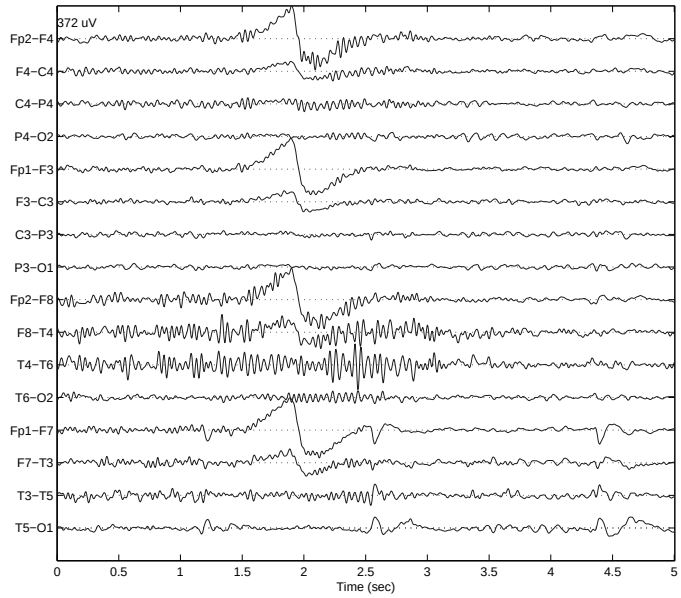

Figure 2.2: An artifact caused by an eye blink between 1.5 and 2.5s

Pulse artifact The pulse artifact is responsible for a pulsating, quasi periodic signal that happens between two ECG R waves. This happens when electrodes are placed over a pulsating blood vessel. It can be identified by observing the EEG synchronous with the ECG. This artifact becomes significant when the EEG is captured inside a high magnetic field, like during an fMRI scan. This artifact will be further explored in this thesis and methods for its removal are reviewed and a new method, based on its physiological source is proposed and evaluated.

Skin The skin can also be a source of distortion of the EEG. Because its impedance is not constant depending on different factors like sweat, different amplitudes can be recorded depending on the current skin properties.

The non-physiological sources of artifact, can be caused by the electrode, when it pops out, or due to electrical interference in the EEG electric wires. These are caused by the alternating current artifact (50//60 Hz) present in power lines, by changing magnetic fields in the environment, like during fMRI sessions, which cause high amplitude and frequency artifacts that obscure the underlying physiological EEG. Radio transmitters placed close to the patient can also be a source of artifact (cell phones).

Combinations of both kinds of artifact can happen when physiologically caused movements

are combined with external magnetic fields. In the case of the previously referred pulse artifact, the physiological causes, cause very small movements of the electrodes, that, being inside a magnetic field, artifacts are generated.

2.6 Summary

The EEG is one most reliable techniques to directly observe the brain dynamics. It is a standard tool for the study of various conditions like epilepsy where the high frequency brain activity is measured. However, it is subject to various artifacts that interfere with the underlying brain activity signals, so techniques to remove those artifacts are needed. Its spatial resolution is also limited, so the integration with complementary techniques has been the focus of various studies. In this thesis we explore its simultaneous use with functional magnetic resonance imaging techniques.

Chapter 3

Magnetic Resonance Imaging

Any sufficiently advanced technology, is indistinguishable from magic.
Arthur C. Clark

Magnetic Resonance Imaging is an imaging technique that allows a non-invasive observation of rich in hydrogen bodies[1]. It relies on the physical principles of Nuclear Magnetic Resonance[2]. The original idea was presented by Dr. Raymond Vahan Damian in 1969 who was also awarded the very controvert Nobel Price of Medicine for its invention. The first human scan was achieved in 1977 by Dr. Damian together with his colleagues Dr. Larry Minkoff and Dr. Michael Goldsmith, taking almost five hours to generate one single image. The scanner built for this experiment was named *Indomitable* to transmit the struggle for something that seemed like magic or impossible to achieve[53].

3.1 Spin Physics

The physical property that is explored in Nuclear Magnetic Resonance is the nuclear spin (Fig 3.1). It is an intrinsic quantum number and cannot be changed under any known circumstance. Its only two possible values are -1/2 or 1/2. Because it's spinning and the particles distributed mass, it possesses an angular momentum. This way the axis of rotation is retained. As a spinning electrical charge, the particle also has a magnetic moment B, behaving like a tiny magnet, susceptible to be influenced by external magnetic fields. When a particle is placed in a Magnetic Field, it's tendency is to align itself with it, in a precessional motion. Because of its spin, the alignment happens with a precessional motion (Figure 3.2).

[1] Fortunately, most living organisms are constituted by water

[2] The *nuclear* word has been removed from the name because of the negative associations that existed for it that time

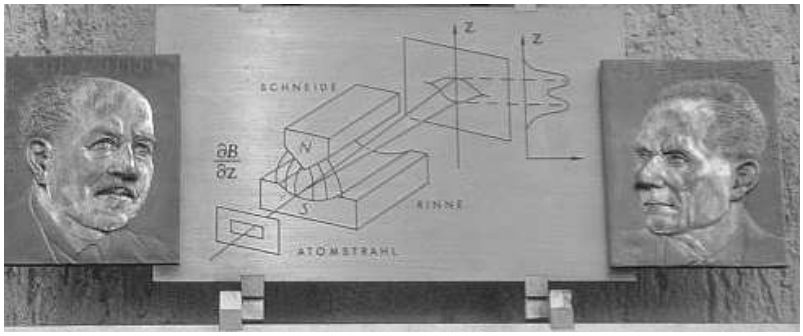

Figure 3.1: The Stern-Gerlach experiment: In 1920, two German scientists have experimentally confirmed the nuclear spin. Otto Stern and Walter Gerlach shot a beam of silver atoms through a highly non-uniform magnetic field. Instead of finding a uniform projection, they observed two positions where the silver accumulated, suggesting two opposite spin directions.

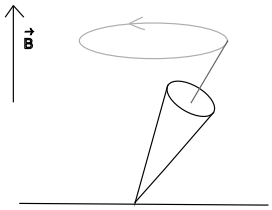

Figure 3.2: **Precessional motion:** An analogy with a spinning top can be used at this point. When a spinning top slows down as a consequence of friction, the force of gravity starts acting on its sides, making the spinning top become more and more inclined in a precessional motion until it finally falls. In atomic particles, the spinning speed is always constant, however, the precession speed varies with the external field strength.

This motions frequency is directly proportional to the external magnetic field strength and is called the Larmour Frequency:

$$\omega_0 = \varphi * B_0 \tag{3.1}$$

Where ω_0 is the Larmour frequency (MHz), φ the gyromagnetic ratio (MHz/T) and finally B_0 the magnetic field strength (T).

This alignment occurs because the nuclei *prefer* to be in the lowest energy state. However, because of thermal energy, not all nuclei align in the parallel direction[3]. Nonetheless, the quantity of parallel aligned nuclei is proportional to the field strength. At this point the

[3]This total alignment would only happen at a 0 K, which isn't a very comfortable acquisition temperature for in vivo imaging

system is considered to be in a stable state. The Nuclear Magnetic Resonance phenomenon occurs when a perpendicular electromagnetic wave, with the same energy as the Larmour frequency acts on the nuclei, thus *resonating* at the excitement frequency (Figure 3.3).

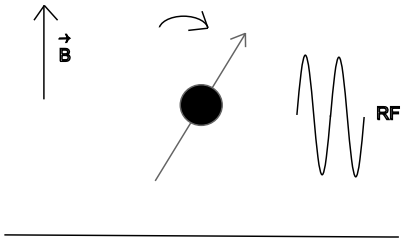

Figure 3.3: **Magnetic Resonance**

This causes the M vector to gradually incline, making the nuclei precess around B_0 in phase with the electromagnetic wave until it reaches a 90 degrees angle. In this position, the particle is *excited*.

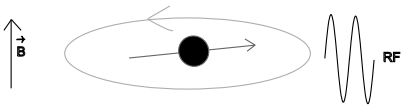

Figure 3.4: **Extited particle**

3.2 T1 and T2 Relaxation

At the moment the excitation wave ceases, the nuclei gradually return to it's lowest energy state. This is called the *relaxation*. During this process, two independent phenomenons can be observed:

Spin-Lattice interaction (T1 relaxation): Since the nuclei gradually align with he external magnetic field, its magnetic vectors sum up in the direction of B_0 with a T1 time constant until it reaches the equilibrium. In this process energy is released in to the surroundings[4]. Bloch has predicted that thermal fluctuations would cause the longitudinal magnetization to be restored at an exponential rate:

$$M_{longitudinal} - \varphi B_0 = exp(\frac{-t}{T1}) \tag{3.2}$$

[4]spin-lattice interaction

This time constant T1 is independent of the B_0 field strength and of any interaction with other particles.

Spin-spin interaction (T2/T2* relaxation) Just after the transverse wave ceases, all nuclei are rotating in phase. This makes the magnetic vectors sum up, Thus inducing an alternating current at a transverse receiver to B_0. However, because of nuclear interactions a dephasing phenomenon occurs, causing the magnetic contributions to cancel each other out until all nuclei precess with a random phase.

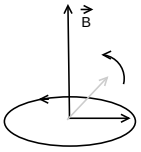

Figure 3.5: **T1 relaxation**

This decay of transverse magnetization happens with a characteristic time constant: T2.

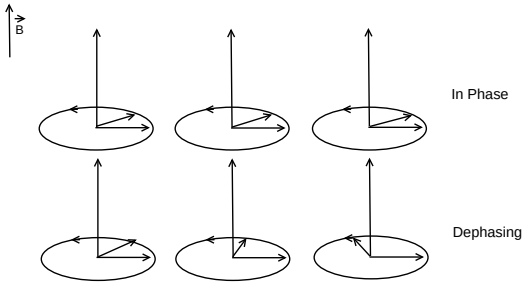

Figure 3.6: **T2 relaxation**

Because of field inhomogeneities in the B_0 field, and the body being imaged, the signal will not decay with the time constant T2 but with a rather faster decay T2*. This field inhomogeneities that accelerate the decay, can be compensated by applying a 180^o pulse. The magnetic field decay, can be described by:

$$M_{transversal} = exp(\frac{-t}{T2}) \tag{3.3}$$

It is important to note that the two above described phenomenons happen simultaneously but are totally independent of each other.

3.3 Imaging

Magnetic Resonance Imaging provides us with tomographic images of the studied body. In the following subsections a brief description is provided of how the imaging is achieved by using the above described physical phenomenons.

3.3.1 Longitudinal encoding

As referred in the last section, the precession angular speed varies linearly with the magnetic field strength. This way, if a magnetic gradient is created and the body is submitted to it, each proton will precess with a different speed depending of its spatial position. This is the basic principle of MRI spacial encoding. By submitting the body to this gradient, each *slice* can be uniquely identified by its frequency. However, we still have two more dimensions left to encode.

3.3.2 X-Y encoding

The encoding in the X and Y direction is achieved by using the frequency and phase respectively. This way each *line* in the Y direction is uniquely identified by its phase and each line across the X direction is identified by the frequency. The phase encoding is made by creating a gradient in the Y direction so each proton along this line will precess at an incremental speed. This causes a dephasing phenomenon. After this gradient is switched off, the precession speeds return to its initial value but the phase difference is maintained, allowing us to identify each Y position by it's phase.

3.4 The scanner

The MRI scanner needs to be able to set the specified magnetic fields very precisely and also measure the emitted signals. This requires a set of components:

Main Coil generates the main static magnetic field allowing the nucleus alignment along its directions. It's typical values range from 0,1 to 7 Tesla.

Gradient Coils These coils are placed along the three coordinates. Their function is to generate the necessary gradients to allow a spatial encoding.

Transmitter Coil This coil is used to emit the RF electromagnetic waves that are used to excite the nucleus.

Receiver Coil The function of this element is to receive the MR signals generated by the resonating nucleus.

One of the most challenging issues in the scanner is to create a strong stable and static magnetic field. There are basically three approaches to create the strong static magnetic field:

Permanent Magnets The greatest advantage of this approach is the no need for a power supply. However, the installation is very difficult because of its weight. They also rely on a constant temperature to maintain a constant field and, in case of an emergency, these cannot be switched off. The typical field strength achieved with these magnets is about 0.5 T.

Resistive Magnets This solution works as a "regular" electromagnet. It is a much lighter solution than a permanent magnet and can be switched off quickly. However, as it is resistive it dissipates huge amounts of energy and relies on a constant current to achieve the desired homogeneity of the magnetic field.

Superconducting Electromagnets Modern scanners are equipped with superconducting electromagnets. These are made of niobium-titanium alloy, that behaves as a superconductor when submitted to a 4K Temperature. To achieve this temperature, liquid helium is used, which must be constantly supplied. However, because a superconductors resistivity is effectively zero, once the field is established it remains constant. This approach allows the generation of field strengths up to 18T.

3.5 Functional Magnetic Resonance Imaging

MRI provides a good resolution, non invasive anatomical visualization tool. The images achieved are based on the contrast derived from from tissue relaxation parameters T1 and T2. It can be used to visualize several conditions like tumors or anatomical disorders. Because of the relative high speed the T2 parameter can provide, high speed acquisitions can be configured. This allows one to have a time-line of volumes and the study of the differences between them. This section describes how MRI is used to dynamically study the brain function.

The brain function can be indirectly measured by the increased blood flow into the active region, and also the greater oxygen consumption. This principle is used in the most commonly used to study the brain function, and is called BOLD-fMRI (Blood Oxygen Level Dependent fMRI). Other imaging like the Single photon emission computed tomography (SPECT) and the Positron emission tomography (PET) use the emitted energy from injected radioactive

particles to observe the increased blood flow. fMRI provides several advantages over these classical techniques. Since it is non-invasive, and does not involve the injection of any substance, a patient can be repeatedly imaged, allowing the application of statistics to distinguish between a subjects different mental states. Because of its low risk, imaging on healthy patients and children can be safely performed. Other fMRI modalities include *perfusion fMRI* which measures regional cerebral blood flow, *diffusion-weighted fMRI* which measures random movement of water molecules, and MRI spectroscopy which can measure certain cerebral metabolites noninvasively. In this thesis only the BOLD-fMRI will be further explored since it is the modality used on EEG-fMRI studies.

3.5.1 BOLD-fMRI

Using fMRI the brain function can be indirectly measured because of the hemodynamic response. Active nerve cells consume more oxygen, so the hemoglobin gets deoxygenated in the places where the brain is active. Also, there is a greater blood flow in the active region. This response starts with a 1-5s delay, and has a peak around 4-5s[38]. fMRI is used to

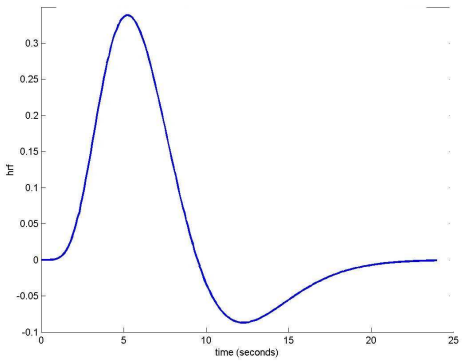

Figure 3.7: The hemodynamic response measured from the stimuli at 0s. The peak of the hemodynamic response is around 4-5s

explore these changes because hemoglobin has different magnetic properties depending of its oxygen level: When oxygenated (oxyhemoglobine) it is diamagnetic while when oxygenated (dyoxyhemoglobine) it is paramagnetic. This signal will be stronger for the brain areas where the oxygen consumption is higher, thus providing us an indirect way of measuring the brain function. Tho achieve this image difference, T2*-weighted images are performed. Because the deoxyhemoglobine properties cause it to dephase faster than the oxyhemoglobines, the T2* signal is retained longer for the regions which have more oxygenated blood. This way, a region with more oxygenated blood will show brighter on T2* weighted images. Spin echo

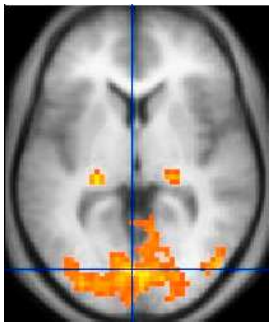

Figure 3.8: Sample fMRI data with an anatomic reference

sequences can also reveal the BOLD contrast because of diffusion effects. However, for research purposes the most common sequence is the EPI sequence because it provides fast acquisition rates, thus allowing to detect short stimuli[12]. In order to carry out experiments using fMRI, the subject must be repeatedly stimulated and continuous brain imaging is required. This way, the success of the experiment is dependent of three factors: the scanning sequence, the design of the stimulus paradigm and the way the data is analysed(Figure 3.8).

3.5.2 fMRI analysis

The next step after acquiring the raw data from the scanner is its analysis. The main goal in fMRI analysis is to find the regions where the signal changes upon stimulus presentation. Also, the degree of confidence that we can place on each previously calculated voxel should be considered for a successful analysis. The choice of the appropriate statistical test, depend on the the assumptions that can be made and the addressed questions in the test. To determine the significance of the given results, multiple comparisons are performed and the reduction of freedom degrees result in smoothing. The most robust algorithms for finding the activated areas, rely on finding, for each individual voxel, a temporal response that matches an a priori expected model. A new approach using model free analysis calculates the correlation between every single voxels time series. This of course is very computationally demanding, so innovative high throughput computing architectures are being used to address this problem. The results from this analysis provides us with the Statistical Probability Map (SPM), which shows us the probability of each voxel being active. Still, one more important operation is necessary before presenting the analysed data. Statistical Inference should be applied in order to highlight only the pixels that show with a high degree of confidence the localization of active pixels. This is achieved by threshold the SPM data. The result of this analysis is a map of the most probable activated areas.

3.6 Summary

Magnetic Resonance Imaging has become a breakthrough technology in the study of the human body. Its molecule level non-invasive nature allows the observation of subjects without known side effects. The fMRI technology allows a dynamic observation of the brain, however it is far from becoming as fast as the highest frequency brain activity, limiting its use in observations where these dynamics are of great importance like in epileptic patients. Thus further investigation in the integration of this technique with other capable of recording the high frequency dynamics is of great importance and has become the main motivation for this thesis.

Chapter 4

EEG-fMRI

Great things are not done by impulse, but by a series of small things brought together.
Vincent van Gogh

Functional Magnetic Resonance Imaging (fMRI) is a technique that allows monitoring of the brain activation patterns by measuring the magnetic variation induced by changes in the blood flow associated to brain neural activity. As explained in the MRI-fMRI chapter, the neural activity produces an increase in blood flow (with a delay of about 2 seconds) richer in oxyhemoglobin to compensate the increase in oxygen consumption. This change in oxyhemoglobin is called the Blood Oxygen Level Dependent response or BOLD effect [37]. The local fluctuations in BOLD induce magnetic variations are susceptible to be detected through T2-weighted gradient-echo echo-planar imaging [13]. When BOLD activations and deactivation are time related with specific events, they can be related to metabolic response in the brain. Therefore fMRI provides an indirect way of studying the brain activity [13]. Although it provides a good spatial resolution, the drawback of fMRI is its poor time resolution (typically an head volume acquisition every 3 seconds in a 1.5 T MRI machine), a limiting factor when observing the rapid brain electrical dynamics. However, these can be reliably characterised through the electroencephalography (EEG) where electric potential variations, induced by electrical brain activity, can be measured on the scalp surface in high sampling frequencies ($\geq$ 200Hz). But in contrast to the ability of capturing events in real time, EEG has a limited spatial resolution. Integrating both techniques (EEG-fMRI) represents an added value both in normal and abnormal brain activity characterisation [43]. This integration is not free from problems due to artifacts induced in EEG by magnetic field variations: EEG relies on cables connected to the subjects head to capture the electric potential over the scalp that, when acquired inside a MRI shielded room, are subjected to electric inductance generated by

the very strong static and varying magnetic fields in fMRI sequences, thus strongly obscuring the original EEG signal. In this environment the two most relevant artifacts are: the imaging artifact originated by magnetic field gradient fast alterations and the Ballistocardiogram (BCG) induced by heart pulse[43].

4.1 EEG-fMRI acquisition protocols

To obtain a usable signal both from EEG and fMRI, the must adopt strategies to overcome the problems in combining these modalities. The induced artifacts on the EEG signal obscure the signal, so the EEG is either an alternating approach is used where EEG and fMRI are not continually acquired, or Artifact removal techniques must be applied.

4.1.1 EEG-Triggered acquisition

In order to avoid the Gradient artifact, the scanning can be trigged to start only after an EEG event has been observed. Since the bold response takes a few seconds to reach it's highest value, the fMRI response has a delay that can be used to start the scanning after the EEG event has been observed[52][46][29]. This interleaved recording approach has been widely used in the first simultaneous EEG-fMRI acquisitions[19][30], however it presents several disadvantages and problems:

- The EEG must be continuously observed by an experienced technician who must activate the scanning right after an event has been observed. The low

- Low frequency drifts can not be taken in account

- An equivalent number of baseline frames and post event frames should be captured. This causes additional difficulty since while scanning the EEG cannot be observed. Thus one can never be certain that the baseline captured frames aren't actually post event frames. To overcome this problem the injection of short-acting anticonvulsants has been proposed. This approach can be useful in patients with a high spiking rate, however it can change the cellular metabolism, and consequently difficult the interpretation of the results.

- The EEG is still *contaminated* with inside the scanner movement and pulse related artifacts that difficult even further the interpretation of the results.

4.1.2 Continuous EEG-fMRI acquisition

The continuous acquisition of EEG and fMRI presents many clinical advantages over the EEG-triggered acquisition. Besides solving the above stated problems, it opens new opportunities to relate the EEG and the fMRI response. Not only spikes can be used to study the localization of the brain activity, but also other EEG events such as the Breinshalf potential.

The use of continuous acquisitions of simultaneous EEG and fMRI requires the removal of the artifacts from the signal to make it usable for use by clinicians. For this step to be successful, the acquired signal should not be saturated, as it must contain the combined underlying physiological EEG together with the induced artifacts. Thus, the amplifier must posses a large dynamic range because of the high amplitude gradient interference. Following the acquisition, the artifacts must be removed as they obscure the original signal. In the following sections, we explore the two most common artifacts present in the EEG-fMRI simultaneous acquisition: The Gradient related artifact, and the pulse related artifact (Ballistocardiogram).

4.2 Real time EEG-fMRI acquisition

The early interleaved EEG-fMRI attempts to simultaneously record EEG and fMRI were by it's nature done in real time. A continuous monitoring of the EEG was necessary to trigger the scanner in order acquire the fMRI following some event. Most of the continuous acquisition techniques rely on the off line EEG signal processing to achieve a clean signal. Garreffa et al.[18] has reported the implementation of a system that allows a control of the electrophysiological behavior of the patient during an fMRI scan. They performed a detailed analysis of the gradient artifact wave-shape to create a good model of the induced signal. Specific algorithms were tested to remove the Ballistocardiogram artifacts and were mainly based on AAS. The reported setup was tested on a Pentium III 800MHz processor with sampling frequencies up to 4 kHz. This demonstrated the possibility of real time EEG-fMRI monitoring during the gradient sequences. With modern computers, more elaborate algorithms could be used.

4.3 EEG artifacts in EEG-fMRI

The scanner room is a very hostile environment for any electrical device because of the strong magnetic fields the devices get exposed to. Induction phenomenons happen when a wire is exposed to a varying magnetic field. This variation can be observed in two situations: A wire moving inside[1] a static magnetic field, or a static wire subject to varying magnetic fields.

[1] In a perpendicular direction

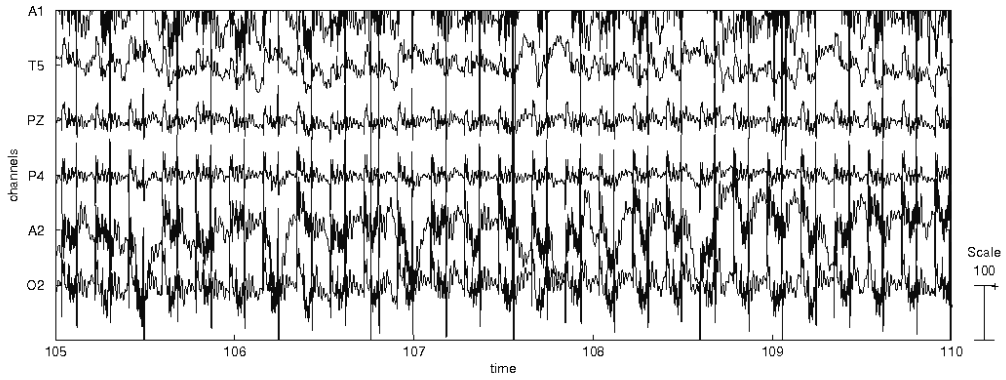

Figure 4.1: Sample EEG recorded during scanning. The underlying EEG gets completely obscured with the induced artifacts

In the MRI scanner we find both situations giving rise to two characteristic artifacts. The varying magnetic fields found during scanning give rise to the **gradient** artifact (Figure 4.1), and the strong static magnetic field is the main responsible for the pulse related artifact, the **ballistocardiogram** (BCG).

Several approaches to the removal of these artifacts have been presented. To achieve a successful method for this goal, we need to understand the signals, so in the following sections a description of these artifacts is presented, followed by a description of the most common methods for its removal.

4.4 Artifact Removal in EEG-fMRI

The removal of EEG artifacts found in the simultaneous acquisition of EEG and fMRI has been a great focus of research because of the advantages and potential this method presents for various medical diagnosis.

Most of the artifact removal techniques fall into one of following categories: Frequency filtering, independent component analysis and average artifact subtraction. A common assumption to most of the proposed methods is that the resulting EEG can be modeled as an addictive system, consisting of the physiological EEG, with the added gradient artifact, ballistocardiogram artifact and noise. It is safe to assume the independence of the Gradient artifact and the physiological signals. With the Ballistocardiogram, this assumption is not so obvious, however the effects that could contradict this assumption are very small. Therefore, the resulting signal can be described by:

$$y(t) = p(t) + \sum g(t) + \sum c(t) + \sum n(t) \tag{4.1}$$

Where $y(t)$ is the resulting EEG, $p(t)$ the underlying physiological EEG, $g(t)$ the gradient related artifacts, $c(t)$ representing the pulse related artifacts and $n(t)$ the noise.

4.4.1 Frequency filtering methods

The most straightforward method to remove or attenuate an artifact on a signal is by filtering it in the frequency domain. Frequency filtering is basically achieved by transforming the signal into the frequency domain, removing the unwanted frequencies. Finally, a transformation back to the time domain is performed resulting in a signal with the unwanted harmonics removed. If some artifact has a well defined frequency range, and does not overlap with the signal frequency, it can be safely removed without distorting the underlying signal. Otherwise, simple filtering will always distort to some degree the underlying signal. Because signals are not constant over time, adaptive filtering allows the filter parameters[2] to be dynamically adjusted depending on the current signal characteristics.

4.4.2 Average Artifact Subtraction

Average artifact subtraction is a method to remove repeated patterns, with a well defined position from a signal. By this means, if we average repeated random pieces of the signal with the same length, the resulting signal will gradually stabilize into a constant wave-shape. This way, if some pattern is added to the signal repeated times, one can estimate it by averaging the aligned signal portions containing the pattern. Two assumptions are made to achieve this goal. First, the signal mean must be constant (or zero, if we don't take in account the DC component), and second, we must precisely know the added pattern positions. There are many possible variations to this method which will be further explored in the following chapter. Prior to subtraction, the averaged artifact can be weighted if there are known variations on the amplitude, or it can be "stretched" or "compressed" in the time domain to match the possible time variations. This method is covered in detail later in this thesis where we present an evolution of this algorithm, by dynamically adapting the artifact in the time domain to the underlying signal.

4.4.3 Independent Component Analysis

Independent Component Analysis (ICA), aims to recover independent sources from a set of simultaneously acquired signals that result from a linear mixing of the source signals [14]. In

[2] the filter kernel

such configuration, we have a set of signals, each one of them contains the linear mixture of a set of different sources. In every signal, all the sources are present, but with different weights. The goal of ICA is to find the weights of each source on every signal. A classical example used to illustrate ICA is the **Coctail Party** problem. By placing as many microphones as sources of sound in the party, each microphone captures all the sound sources with different amplitudes, depending on the distance to every subject. Therefore, each microphone output, can be seen as a linear mixture of the captured sound. ICA aims in separating every individual source of sound from the sounds captured by the microphones. To achieve this goal, ICA makes the following assumptions:

- Every signal results from a linear mix of the sources
- The source signals are statistically independent
- The source signals do not present a Gaussian distribution
- The number of sources and sensors should be the same

This way, every sensor $y_k(t)$ results from the linear mixture of $x_k(t)$, with the weight matrix W.

$$\begin{bmatrix} y_1(t) \\ y_1(t) \\ ... \\ y_n(t) \end{bmatrix} = W \begin{bmatrix} x_1(t) \\ x_1(t) \\ ... \\ x_n(t) \end{bmatrix} \tag{4.2}$$

Although we can only observe Y, the goal of ICA is to estimate the matrix W that decomposes Y into W. In real world signals, the goal is to find the most independent sources possible, as the measured signals are subject to different factors such as noise. Several methods for finding this matrix exist, which will not be explored on this thesis. The encephalogram can be seen as a linear mixture of various sources as every electrode measures the integrated potential difference from different brain sources at the same time. Not always the sources are independent processes as different brain areas may be working on the same task. However, in the case of the artifacts found in the ballistocardiogram, their source is clearly independent from the physiological sources and so the ICA approach is a potentially good method for the extraction of EEG-fMRI artifacts.

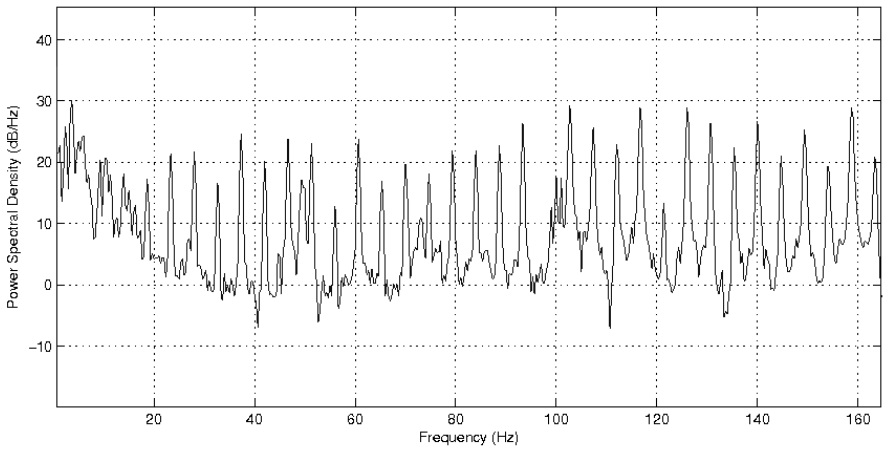

Figure 4.2: Frequency Spectrum of an EEG channel contaminated with the gradient artifact

4.5 The gradient artifact and techniques for its removal

The Gradient Artifact consists of strong perturbations of EEG signals induced by the time varying magnetic field gradient.

This artifact is widespread over the EEG frequency, ranging from 0.5 to 70Hz. Since these frequencies overlap with the physiological EEG signal, simple low pass filtering is not satisfactory to remove the artifact. Felblinger et al.[34], has shown that a fourth order low pass filtering with a cut off point of 13Hz could not suppress this artifact (Figure 4.2).

The EEG gets completely obscured with this artifact, so in order to enable it's analysis strategies must betaken. As explained in the protocols section, interleaved recording [19][30] was the early approach to avoid this problem. The delay in the BOLD response (about 3s), allows an EEG-triggered fMRI acquisition paradigm[29]. However simultaneous recording provides valuable data and in certain cases it is absolutely necessary[50]. Our goal is to study methods to improve the simultaneous acquisition, so this paradigm won't be further explored. This artifact is, in theory, very consistent over time, however the overlapped signal found in the EEG does not always correspond to this perfect scenario. Although the magnetic field that induces the artifact is consistent over time, the overlapped signal found in the EEG can be subject to variations. This changes can be caused by timing errors between fMRI sampling and EEG samples [13], changes in electrode position and orientation over time and mechanical vibrations not in phase with the changing magnetic field. The timing errors can be due the higher frequency components induced in the EEG wires than the typical sampling rate. For the removal of this artifact, solutions based on Average Artifact Subtraction (AAS)

and adaptive frequency filtering have been proposed.

Hoffman et al.[22] has proposed a technique to filter the artifact by taking the frequency spectrum of a base line signal and using it to find the artifact harmonics on a contaminated signal. By taking 10s of signal acquired inside the scanner, free from movement and scanning artifact, they used it as a base signal for the following filtering process. This signal should, if possible, contain the characteristic EEG activity of the patient, like epileptic spikes. The frequency spectrum of this signal is then taken. To filter the artifact of a contaminated signal, the signal is transformed into the frequency domain, and the frequencies where it differs from the baseline, by some factor, are registered. These harmonics are set to zero as they are supposed to correspond to the harmonics of the artifact. Finally the inverse Fourier transformation is taken, resulting in a signal free from the artifact.

Since the gradient artifact is by its nature consistent over time, the most widely used algorithm for its removal is the average artifact subtraction. For this process to be successful, the artifact should be faithfully recorded and remain stable over the scanning period. This implies that the amplifier must not saturate and the signal should be acquired with a sampling rate capable of recording the signal without aliasing effects.

A continuous averaging of the artifact can reveal the artifact wave-shape which can be in turn subtracted from each signal portion that contains it. However, as referred earlier in the text, although the electromagnetic causes are stable over time, the recorded artifact on the EEG may not be. Causes for this are the scanner vibration which may cause the wires to vibrate and slightly change their position, inducing variations to the acquired artifact(1). Also, the sampling rate of the EEG may not be sufficient to faithfully record the artifact(2). Phase variations between the EEG clock and the fMRI scanner clock can also cause aliasing problems in the artifact sampling[13](3). Problem (1) can be solved by using only the last frames for averaging instead of using all of them. The number of frames to average is a compromise between the rate of artifact change and template quality. The typical compromise between the number of averaged frames and template quality is 10[2]. To overcome the pointed (2) and (3) limitations, Anami et al[4] used a single clock to synchronize both the EEG and fMRI and modified their gradient sequence to get periods with low artifact amplitude. Goldman et al.[19] suggested acquiring the EEG time locked to the fMRI acquisition, thus allowing a lower sampling rate. These approaches have proved to be very effective, Although modifications in the EEG and fMRI systems are not always possible. When the sampling rate is not sufficient to record the gradient artifact, aliasing effects may happen when recording the EEG. So, depending on the phase am artifact starts being sampled, its acquired wave-shape will vary. An approach to overcome this limitation is to divide the sampling period into bins (usually 10). Then, each acquired artifact is placed on the respective bin, depending on the

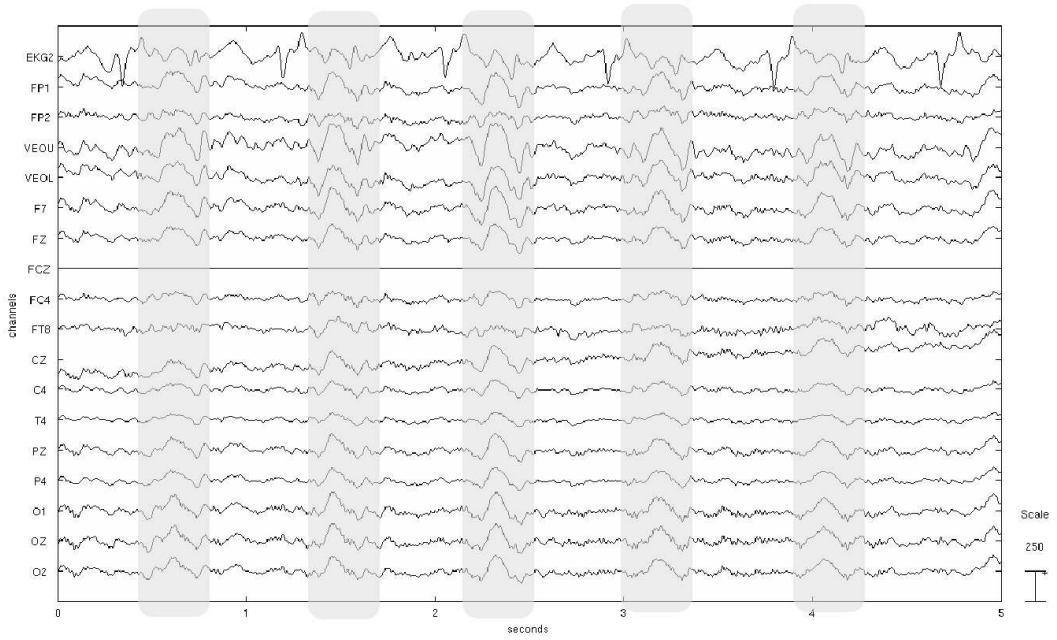

Figure 4.3: Sample EEG with BCG artifact

phase at which was acquired, simulating a sampling rate 10 time higher. This approach allows a lower sampling rate and does not require the use of a trigger from the scanner.[6]

The removal of the gradient artifact provides clinicians a readable signal. At this point, the signal although still contaminated with the ballistocardiogram artifact reveals a closer signal to one acquired without the influence of the magnetic fields.

4.6 The ballistocardiogram

The Ballistocardiogram (BCG) artifact (Figure 4.3) occurs between two successive ECG R waves, and so it is associated with the subjects pulse. The causes for its occurrence have been the subjects head motion, the expansion and contraction of the scalp arteries in the static magnetic field and the Hall effect when hemoglobin flows perpendicular to the static field[2, 21, 34, 48]. This last source is believed to be very small, because of the approximate equal number of positive and negative ions in the circulation, and the random blood vessel distribution, that leads to a cancellation of the induced signals [7][44].

This signal has a typical frequency range in the 4-12 Hz frequency band and it's amplitude often exceeds 150μV at 1.5T, that is much larger than the typical alpha activity (50μV)[7] (Figure 4.4). Because of its typical frequency range, it obscures the alpha activity, and

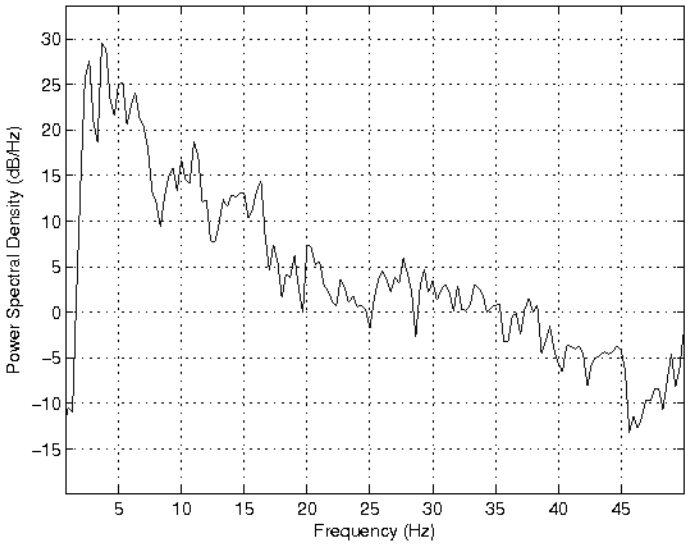

Figure 4.4: Frequency Spectrum of an EEG channel contaminated with the BCG artifact

difficults the identification of delta activity (0.5-4Hz) in sleep studies.

In order to investigate the amplitude, frequency of occurrence and distribution on the scalp, Allen et. al[2]. has performed an experiment to determine these parameters. They used 19 electrodes with the 10/20 EEG system, using strips of electrodes with the leads both twisted and untwisted. The results from this experiment yielded an average 58μV Mean Peak Amplitude for the untwisted leads and 36μV for the twisted leads. The mean distance from the R peak in the ECG channel and the BCG peak was of 0.21s, with values varying from 0.15s to 0.24s. The mean R-R distance was 0.98s, ranging from 0.77s to 1.54s. They referred very small variations for each subject (+- 0.04s), and this value was independent from the R-R variation. The artifact distribution revealed that the BCG was consistently larger in channels with frontal-polar or frontal-central electrodes.

Nakamura et. Al.[35] has presented an experiment that aims to isolate the BCG signal from the underlying EEG. In order to achieve this end, a layer of conducting gel was applied to an insulating sheet that partially covered the subjects scalp. Then, two electrodes were positioned on the gel-covered insulating sheet. With this setup, the electrodes were subject to the exact same sources of artifact found in a regular EEG-fMRI acquisition, but were isolated from the scalp, so the underlying EEG was not recorded. The data was acquired both with and without a vacuum cushion, a setup which allowed to study how the heart beat influenced the head movement. The data was sampled at a 1000Hz sampling rate. This method allowed a good approximation of the BCG without the underlying physiological EEG, so the artifact

could be effectively characterized.

4.6.1 Methods for the Ballistocardiogram removal

Since this artifact obscures the underlying physiological EGG, methods for its removal have been proposed. The proposed methods rely on different techniques such as average artifact subtraction(AAS), Adaptive Filtering and independent component analysis(ICA)[49][8][35]. Bonmassar et. al.[7] proposes a method to remove the BCG artifact based on the principle that the most significant contributions to the artifact are due to small movements in the scanner. These can be quantified by using a motion sensor in a target position on the subjects scalp. An adaptive noise cancellation algorithm was used and the system was modeled as a linear combination of the physiological contributions with the induced artifact. The artifact components are calculated based on the motion sensor output, producing a Finite Impulse Response (FIR) filter kernel. This filter in turn, is used to estimate the noise signal that is subtracted from the acquired EEG. Although this method presented good results its setup is not trivial as it requires a motion sensor.

The most widely used method for BCG removal is the one proposed by Allen et al.[2] and relies on estimating the artifact wave shape by averaging several artifacts, followed by the subtraction of the averaged artifact template to every position. To determine the window position and its length, Allen et. al., has calculated, as explained above, the mean distance between the EEG R peak and the BCG peak, and centered the window on this position, with a +- half the R-R interval for the study group. They used the last 10 ECG intervals to average the template, as a compromise between the time needed to separate the BCG from the underlying EEG and the artifact variations over time. This method performs well in the presence of rhythmic stable BCG induced by basal resting cardiac activity. However, since this artifact results from the subjects physiological responses, to assume this signal is deterministic seems like an unrealistic approach[35]. Sijbers et al.[48] addressed this problem and proposed an enhanced version of this algorithm by, prior to template averaging, time scaling the artifacts to a fixed time interval. Each artifact is then normalized with respect to mean and standard deviation. Also, it is subjected to a wavelet filter where the wavelet coefficients of the highest frequencies are set to zero. The resulting signals are put in a matrix where each column is median filtered. The rows in the matrix are averaged, resulting in an artifact template, which is subtracted to the current EEG epoch. Although a variation in the artifact is assumed, it is still deterministic because it results from a linear wave shape variation, proportional to the R-R distance. This leaves no room for spontaneous wave shape warps, very common in physiological signals.

Mixed methods for removing the BCG have been presented. Kim et. al.[27] presents an

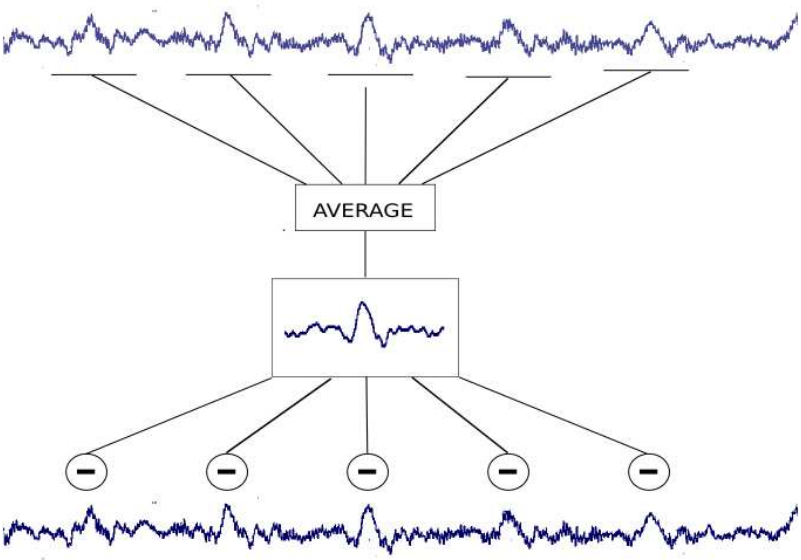

Figure 4.5: **Average Artifact Subtraction**: Assuming the EEG results from a linear combination of the scalp potential with the BCG, and that the EEG mean value is zero, averaging several EEG portions on the artifact positions, reveals the underlying artifact. This averaged artifact is subtracted from the EEG on the BCG positions

algorithm that combines mean subtraction and adaptive filtering. Wavelet post-processing is also used for removing residual pulse artifacts. However, as they refer, the assumption that the BCG is quite stable, is not correct, and thus the need of post-processing methods for removing the remaining artifact. The EEG distortion caused by an improper adaptation of the signal and the template in AAS isn't taken in account and the post-processing methods rely on the principle that there exists the underlying physiological EEG and residual artifact. The basic assumptions described above, that the BCG is a linear contribution to the overall EEG signal, present ICA as a good potential algorithm to find the BCG related components. After separating the signal into independent components, the ones responsible for the BCG can be identified by visual inspection or by computing correlations with the simultaneously acquired EEG channel [49]. A good study of the application of ICA for the removal of the Ballistocardiogram is reported by Nakamura et. al[35]. Although this study showed the viability of using ICA as an algorithm for extracting the BCG, it revealed very small differences when compared to the AAS. As referred, ICA alone could not separate BCGs from EEG completely, what indicates a violation of the ICA assumptions. This indicates that the underlying sources of the EEG data may not be fully independent. Thus, post processing methods were proposed to overcome this problem. Because of the simplicity of the AAS

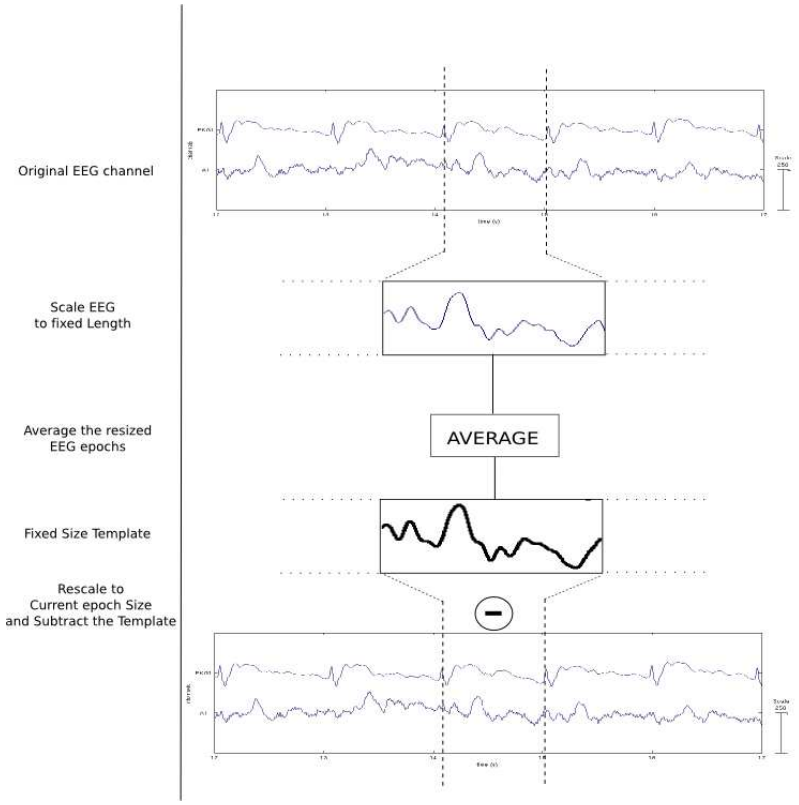

Figure 4.6: Fixed Length Average Artifact Subtraction: The Sijbers et. al. approach to the Average Artifact Subtraction Algorithm: Prior to averaging the artifact, the EEG epoch is scaled to a fixed length. The averaged artifact is rescaled to the epoch size before subtraction

algorithm compared to the ICA, our work will pursue the improvement of the AAS weak points when applied on time varying wave-shapes.

4.7 EEG-fMRI as a tool for the study of Epilepsy

The EEG due to its ability to show abnormal brain activity, is the most influential tool in the diagnosis of Epilepsy. The common trace from patients reveals sharp spikes or series of spikes. These spikes are characterized as ictal (during a seizure) and inter-ictal (occurring between seizures), and can occur in a series of patterns. Those patterns can point the underlying nature of a particular epilepsy type or syndrome.

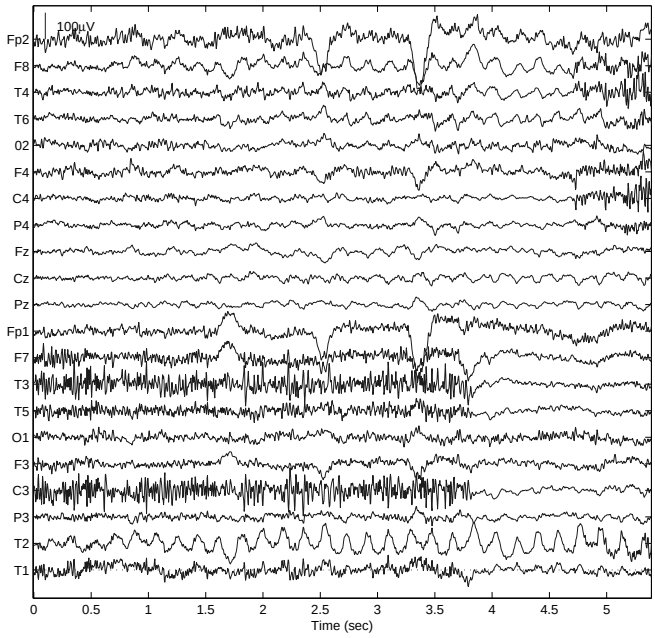

Figure 4.7: A sample EEG showing the end of an epileptic seizure between 3.5s and 4.0s . The high frequency components of the epileptic activity can be clearly observed

Although most Epilepsy cases can be controlled with medication, critical cases exist where patients present uncontrollable seizures. Epilepsy syndromes can be divided into two different categories. Generalized seizures occur on both brain hemispheres and present no defined focus of activity. Focal epilepsy shows a defined brain region responsible for starting a seizure. These cases are targeted to surgery. A pre-surgical evaluation is an essential step towards a successful procedure. During this period, tests are performed in order to identify the seizure

focus, the Epilepsy type and how the seizures relate to other brain functions such as vision or speech. Many times this implies the use of **invasive EEG**. In this procedure, depth electrodes are also a common practice in this pre-surgical tests. During surgery subdural electrodes can be surgically implanted on the brain surface. The referred electrodes can remain implanted during surgery for testing the various brain function and real time checking the affected areas. The goal of the pre-surgical procedures is to localize as precisely as possible the epileptogenic

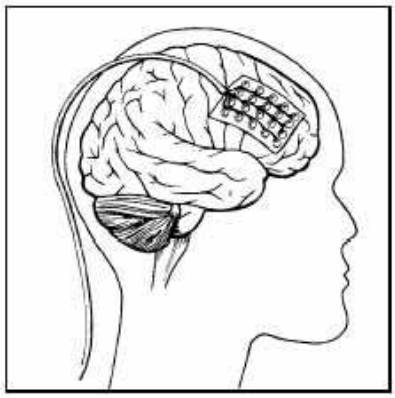

Figure 4.8: Subdural electrode placement illustration

focus. Invasive techniques allow a better spatial focus localization which in many cases is required due to the poor EEG spatial resolution[46]. This low spatial resolution when the EEG is acquired on the scalp surface is due to the signal integration through the various tissue layers in the head. The invasive techniques measure the electrical activity as closely as possible to its source, so an acceptable focus spatial localization can be achieved. This invasive pre-surgical steps can be overcome when the EEG is performed simultaneously with fMRI. While the EEG shows the nature and timing of epileptogenic activity, fMRI can be used to precisely localize its source, improving the precision and the success in the surgical procedure. Another possible application include the use of MRI as an anatomic reference for over imposing functional data. In figure 4.9 we show an example of such an approach where estimated epileptogenic EEG activity sources overimposes a 3D MRI reconstruction of the patients head.

4.8 Summary

Many methods have been proposed for the removal of the Gradient and Ballistocardiogram artifact. The most popular method was proposed by Allen et. al.[2] and, in stable conditions can greatly attenuate the artifacts. However, as it relies on the assumption that the BCG is

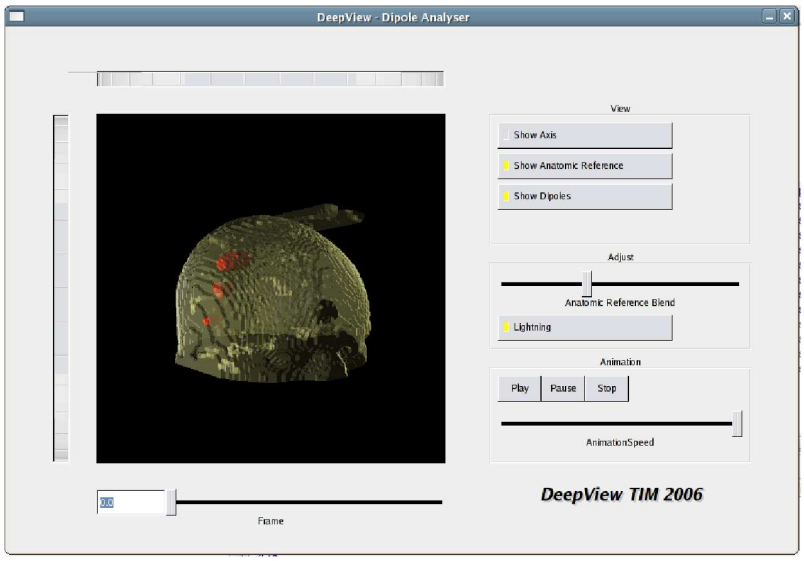

Figure 4.9: The DeepView application, developed by the SIAS group in the University of Aveiro, showing the combined use of EEG and MRI for the study of Epilepsy

deterministic. Being a biomedical signal, it always results in a distortion to some degree. On the following chapter an algorithm that dynamically adapts itself to each artifact is presented, trying to solve the limitation presented by simple artifact averaging.

Chapter 5

A non-linear Dynamic Time Warping Approach to Ballistocardiogram Removal

Things should be made as simple as possible, but no simpler.
Albert Einstein

Dynamic Time Warping (DTW) is a technique for aligning two time series in order to find a dissimilarity measure using nonlinear temporal alignment. This algorithm has found its application in the solution of different problems such as handwriting recognition [32], speech recognition [40]. It's use in the analysis of electrophysiological signals has been of great importance in the analysis of spike patterns [10], event related potentials [51] and in the analysis of the ECG waveform [23]. It provides the ability to compare two time series because it provides an index of the similarity of two time series. In order to calculate this index, the target time series is non-linearly warped into the other, stretching and compressing along the X axis, providing a minimum cost alignment between two time series. It's implementation can become very effective by using Dynamic Programing (DP)[5]. In this problem solving approach, one large problem is divided into smaller problems with decreased level of complexity and since the results from the smaller problems are constantly reused, those are stored to be reused when needed. By using this approach to solve different algorithms, a great boost in performance can be achieved. In this chapter we present DTW as potential tool to improve the effectiveness in the removal of the Ballistocardiogram artifact by not blindly averaging to the template and subtracting it from the signal, but prior to those operations, dynamically warping the signals.

5.1 Method

Supposing we have two time series A and B, of length m and n respectively:

$$A = a_1, a_2, ..., a_m \tag{5.1}$$

$$B = b_1, b_2, ..., b_n \tag{5.2}$$

Our goal is to find which is the best, or lowest cost alignment between the two time series. To achieve this, we build an mxn matrix, where each element corresponds to the euclidean distance between a_i and b_j(5.1). Now, we need to define a warping path that maps the elements of one time series into the other. The warping path W is defined as a contiguous set of matrix elements that defines a mapping between the two time series. Each element of W is defined as w_k:

$$W = w_1, w_2, ..., w_k, ..., w_K \tag{5.3}$$

This path is subject to several constraints:

Boundary Conditions This condition imposes that the warping path starts and finishes on opposite sides of the matrix. So, the first W element corresponds to $w_K = (1, 1)$ and the last element must be $w_K = (m, n)$.

Continuity The path must be continuous. This implies there can be no position skipping, and every path piece must be connected to the previous. Given $w_k = (a, b)$, then $w_{k-1} = (a', b')$ where $a - a' \leq 1$ and $b - b' \leq 1$.

Monotonicity This constraint implies that the path must not turn back, it always increases in one of the permitted directions. Given $w_k = (a, b)$ and $w_{k+1} = (a', b')$ then $a - b' \geq 0$ and $b - b' \geq 0$. On the *optimizations* section some of the possible paths are analyzed.

There are many solutions to this problem, however we are interested in the path that minimizes the cost. In order to efficiently find this, we should divide the problem into smaller subsets that we are easily able to solve. Starting from the target corner in the distance matrix, there is w_k preceded by w_{k-1} which connects to w_k through its lowest cost path. So each W value can be calculated by:

$$W(a, b) = d(A_a, B_b) + min \begin{cases} W(a-1, j-1) \\ W(a \quad - \quad 1, j) \\ W(a, j) \end{cases}$$

(5.4)

Where $d(A_a, B_b)$ corresponds to the distance between A_a and B_b, and min is the minimum cost of the selected paths.

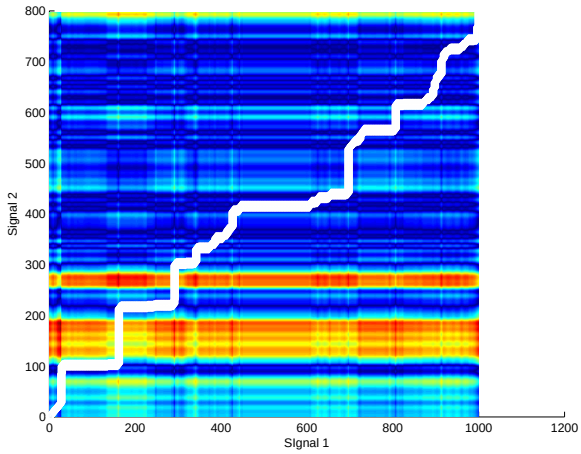

Figure 5.1: A distance matrix showing with the overimposed minimal path

5.1.1 Optimizations

Since the above described algorithm is expensive in computing, it should be subject to several optimizations. The first paradigm used to exponentially increase the calculation speed, is Dynamic Programming (DP)[5]. DP is a mathematical method that is used to solve problems composed of overlapping sub problems. The technique relies on calculating and storing all the previous sub problems so these can be reused when needed. This approach turns many algorithms whose computing time exponentially increases with the problems complexity into linearly increasing time. In the present case, it is applied to DTW by calculating all the distances between the various elements in the time series, followed by a back trace to find the minimum cost path. However, one can avoid calculating all the distances in the matrix, by introducing some more constraints like windowing, slope weighting and step patterns. These optimizations are analyzed with more detail below:

Windowing Since the best path should not be very far from the matrix diagonal, the number of calculations can be significantly reduced if we restrict the admissible warping paths in a defined area around the matrix diagonal (Figure 5.2).

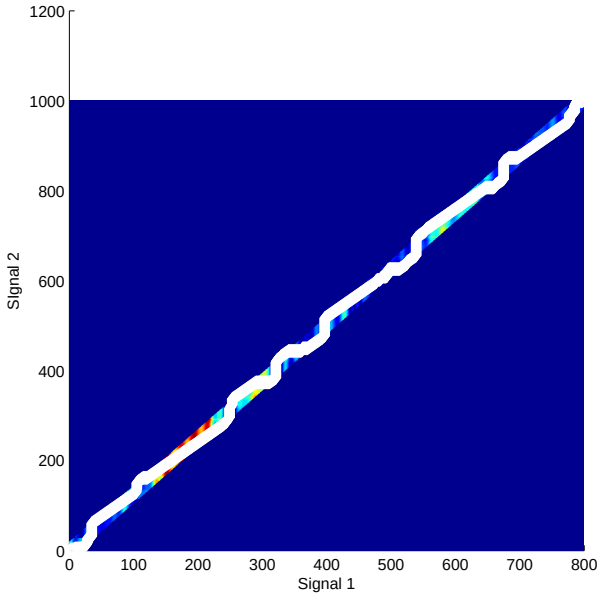

Figure 5.2: A sample distance matrix with a tight windowing restricting the path to the center

Slope weighting Every possible direction for the path to take at each point in time, can be weighted. This way, certain paths are preferable to others. If we consider g_1, g_2 and g_3 as the weights for each one of the steps, then we can generalize equation 5.1:

$$W(a,b) = d(A_a, B_b) + min \begin{cases} g_1 * W(a-1, j-1) \\ g_2 * W(a-1, j) \\ g_3 * W(a, j) \end{cases}$$

(5.5)

Step patterns There can be numerous step patterns defined. The pattern used so far is the equally weighted horizontal, vertical and diagonal pattern. However, this can be adjusted depending on the details of the warping path.

Derivative Dynamic Time Warping Derivative Dynamic Time Warping is a proposed technique to aligned two series that instead of aligning the time series themselves, it uses their corresponding derivative signals to achieve this objective. It was proposed by Keogh et al[26], and it aims in aligning the time series. After performing some empirical

experiences with our data, we have found the results were usually better, so prior to the alignment, our signals were differentiated.

5.2 Applying DTW to the average artifact subtraction

Removing unwanted repeated addictive artifacts in a signal can be achieved by simply subtracting them from the underlying signal. If the artifact wave shape and position is clearly defined, the subtraction is straightforward and the artifact is effectively eliminated. Problems arise when the position, waveshape, waveshape variations in time or all of those are not defined. In this section we explore each associated problem step by step until we finally reach the Dynamic Time Warping approach proposed in this thesis.

If the artifact positions are not clearly defined, one needs to find their position in the signal. This can be achieved by using specific methods for an artifact, using it's unique characteristics or general methods. If the artifact has some characteristic that clearly identifies it, like sharp peaks, it can be identified by time filtering the signal in amplitude, together with its derivative. However, in many cases this is not possible, so a more general and accurate must be used.

Spectrograms provide a frequency vs time graph, so if the artifact shows a distinct frequency signature, it's positions can be identified on the signal. But this is not always the case. Many times the unwanted signals have a close frequency spectrum of the original signal, so it becomes difficult to find their positions with this method.

Signal correlation, is a signal processing operation, that can be described as a comparison of two series at all possible relative positions. Consequently, at the shift where two signals are most similar, a peak will appear. This can be used to find the relative phase of two signals, and also provides a relative similarity measure at all possible shifts. So, if one correlates the known waveshape with the contaminated signal, it will result in correlation peaks at the possible artifact positions. This method is effective if the artifact waveshape is very distinct from the original signal.

Having found the artifact positions, if the waveshape is a priori defined, our subtraction problem is solved as the artifacts are eliminated after this operation. However most of the times the artifact must be extracted from the signal. To achieve this, we must have some a priori knowledge of the underlying signal. If it has zero mean (ignoring the DC component), the continuous signal averaging at random positions, will result in a continuous signal close to zero. This way, if the artifact is added to the signal at random positions, taking its average at the artifact positions, will result in a waveshape that is as close to the artifact as the number of the averaged positions - The artifact template. This method can be used in combination with the correlation, to extract the similar waveshapes from the signal.

When working with biological signals, these are always[1] analog, and not deterministic[9]. This way, the artifact may have variations in amplitude, phase and waveshape. To deal with this variations, we need to adapt the template to the current conditions. The template, prior to subtraction may need to be scaled in amplitude. To obtain the perfect scale for the template, is not a straightforward task, as differences in amplitude in the signal, may be due to the underlying signal and not variations in the artifact.

If the artifact start and end position is defined, and we know the waveshape is linearly warped over time, the template can be "stretched" or "compressed" in the time domain to achieve a better fit. A new problem arises when the artifact has nonlinear variations in the time domain. This happens when the overall waveshape is maintained, but it's phase at each point varies. To solve this problem, the previously described DTW algorithm can be used. When the artifact has a defined position, but it's waveshape is assumed to vary to some degree, like in most biomedical signals, before averaging, and before subtracting, each portion of the signal should be aligned to it's corresponding position (Figure 5.3).

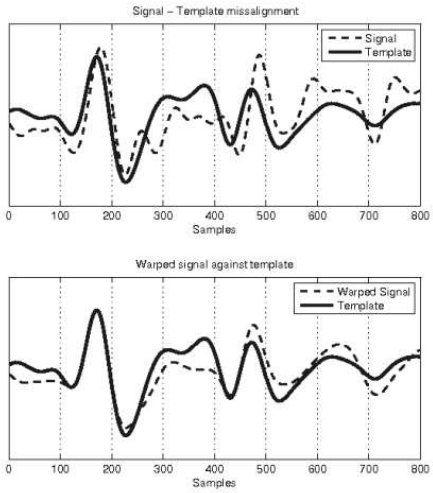

Figure 5.3: An illustration of how DTW aligns a time series to a template

By applying DTW, we can prior to averaging, warp the signal to the target average, obtaining the lowest cost alignment between the two signals. This way, we avoid one portion of the signal averaging with *the wrong* part of the signal. The template achieved by this method, is used, just like in simple average artifact subtraction, to be subtracted to the signal at defined positions. However, prior to subtraction, the template, is warped to match the current signal position.

[1]One discrete signal is in fact present in nature: The DNA

5.3 Implementation Language

To test and implement the above explained algorithms and methods, the selected tool was MATLAB. The considered options are summarized bellow:

Compiled Programming Language (C, C++, FORTRAN, ...) The option to use a compiled programming language, could bring a significant boost in performance. However, this could be part of an optimization strategy after the algorithm has been developed, since extensive testing during implementation is needed, just like programming flexibility and an environment as oriented as close to the user as possible instead of being machine oriented. By taking this in account, using a compiled language like C, C++, pascal to develop an algorithm could take a lot longer and would not provide the needed flexibility to quickly change parameters and paradigms

Scripting Languages (Perl, Python, Rugby, ...) The greatest advantage of scripting languages, is their flexibility to, with a few lines of code, quickly achieve the wanted goal. Also, most of them provide an extensive library choice, and a command line interpreter for instant code execution. The language that way mostly taken in account to develop this algorithms, was Python. This language offers a strong support for integration with other languages and tools, comes with extensive standard libraries and has is open source. This way, it can be freely used, and can run on most known architectures and Operating Systems. However, at the time this thesis work was being prepared, the editor tools available were not yet fully mature, and the lack of good debuggers, an essential tool for the development of algorithms.

Matlab, Scilab, Octava, ... Matlab is a technical computing program, which provides a powerful math engine to compute discrete math. It has a huge amount of libraries associated to it, and most of the signal processing algorithms and it is a golden standard tool for signal processing. It also provides good graphics visualization characteristics which is very useful for representing the data that one is currently working on. It's debugging tools are mature, and provide a real time debugging, with access to command line instructions on the running program data. Although there exist open source clones for it, the needed libraries to manipulate EEG data, like the EEGLAB[15] and the ICALAB[11] were only available and worked properly on MATLAB.

Although MATLAB was selected as the testing and development tool, if the algorithm proves to be successful, and used in a clinical environment, it's implementation in a compiled language should be considered, as in that environment, speed, platform independence and third party software independence is important.

5.4 Implemented algorithms

Our main goal is to test the viability of using dynamic time warping as an intermediate step in the AAS process. Most of the proposed techniques based on this method, are implemented in four steps: Localization, Averaging, Subtraction, Post Processing (Figure 5.4). The algorithm proposed by Sijbers et al.[48] was implemented to compare the results with our approach.

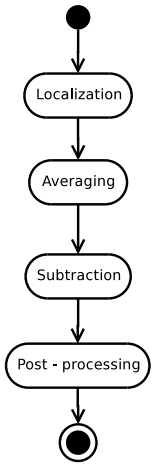

Figure 5.4: The basic steps in average subtraction

5.4.1 Gradient Artifact Detection (Localization)

In order to successfully test our signals, we needed first to remove the gradient artifact. Contrarily to Allen(2000), Sijbers(1999), we did not have a sampling frequency of 5kHz(Allen 2000), nor a trigger signal from the scanner that could help identify the gradient artifact timing, we needed to implement methods that could help us localize the artifacts, and then use this information to apply a simple AAS algorithm.

The AAS approach was implemented to achieve a gradient artifact detection, followed by frequency filtering. This has provided us with a good signal to further process and validate the algorithms for the Ballistocardiogram.

Since we had no trigger signal available that could provide us the time localization of the artifacts, a method based on the Pearsons correlation was developed. Our method requires the identification of a single artifact, which is then correlated through its channel. The correlation results are stored in a signal, in which the maximal are identified and thresholded(Figure 5.5). By doing so the artifacts positions are identified and ready to be averaged and subtracted.

To localize the artifacts positions, we used the correlation of a sample artifact with the

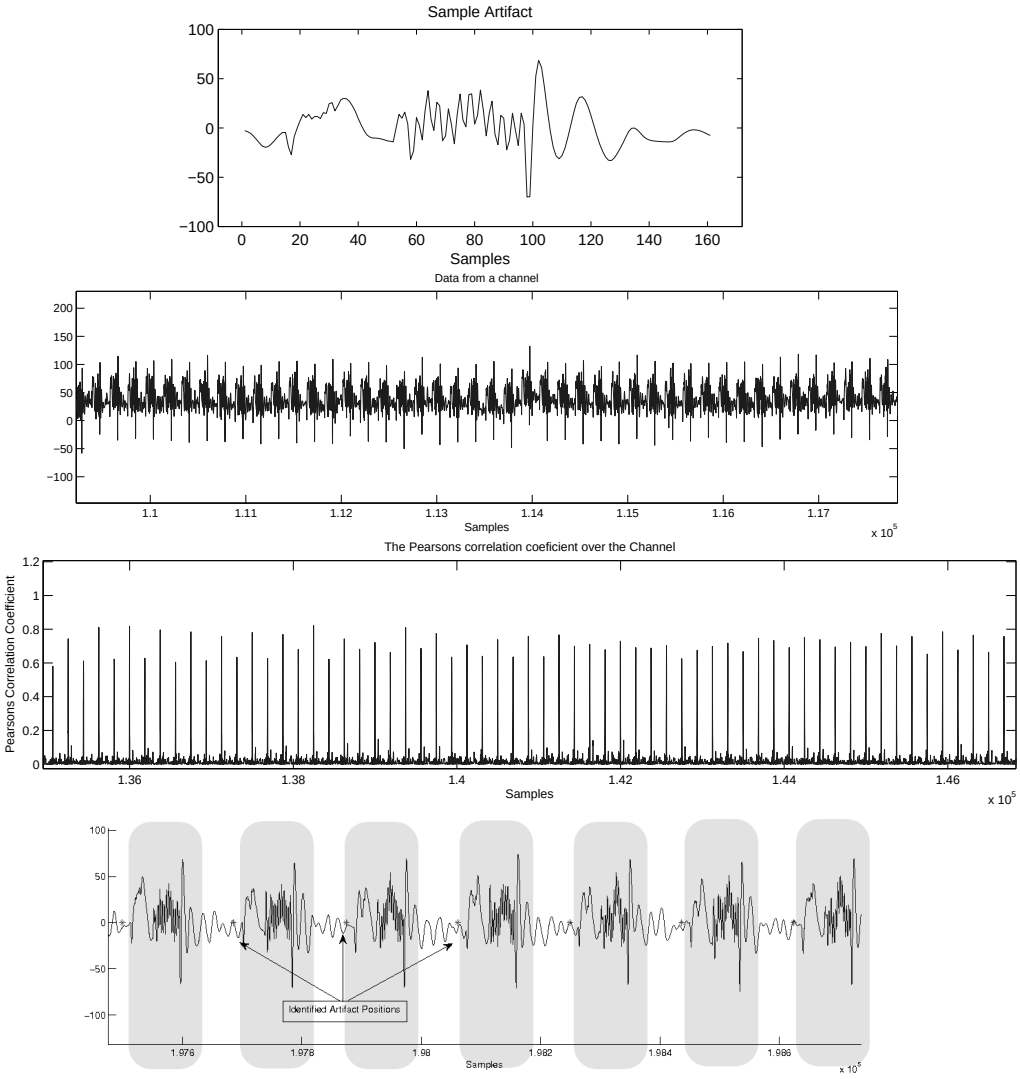

Figure 5.5: The different signals during the gradient artifact detection

signal. Then, this correlation was low pass filtered to remove the close maximal present when passing through a maximal. The max values of this correlation were then used to identify the artifact positions.

5.4.2 QRS detection (Localization)

In order to localize the artifacts positions, the R waves in the QRS complex must be successfully detected. There are many documented algorithms to achieve this goal[28][39][1]. However, because of the bloods conductivity, the acquired ECG inside the scanner suffers from augmented T waves, so simple thresholding methods fail. The FMRIB[36] plugin for the

EEGLAB[15] implements an algorithm that robustly detect heart beats. It uses a combined adaptive thresholding and the Teager energy operator, followed by a correction algorithm. This tool was used to detect the events, followed by a visual inspection and eventual correction. In some signals however, this tool could not detect in a satisfactory way the QRS complexes, so a manual marking was performed.

5.4.3 Average artifact subtraction algorithm

A standard implementation of the Average Artifact Subtraction (AAS), as proposed by Allen et. al[2] was implemented in order to compare our method with the most commonly used. It was implemented to allow the adjustment of the number of artifacts to average, the artifact location and its length. With this arguments the algorithm was flexible enough to allow the reduction of both gradient artifact, and to compare with our proposed enhancement to the algorithm.

5.4.4 Dynamic Time Warping

The implementation details will be provided for the implemented DTW library to be used with MATLAB. Some existing solutions have been tested, however, none provided the desired flexibility to perform the needed adjustments during the testing phase.

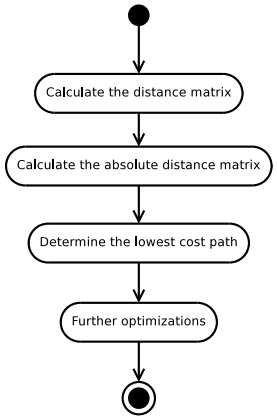

Figure 5.6: The basic steps in the DTW algorithm implementation

Our DTW algorithm was implemented as a matlab function, following the method above described. The code was encapsulated in a matlab function that took as input arguments the source and target signals, windowing optimization size, and a cost matrix. This cost matrix contains the cost of stepping into every direction, and defaults to the standard 1 cost for every three directions (horizontal, vertical, diagonal). The algorithms implementation was

then divided into four steps (Figure 5.6):

Calculate the distance matrix At this step, the distance matrix is calculated. Here, the distance in amplitude of every sample in the source signal, the distance to every sample in the target signal is calculated.

Calculate the absolute distance matrix A second matrix is calculated, starting at the bottom left corner that for every matrix position calculates the distance from the starting point, using the specified cost matrix.

Determine the lowest cost path Given the absolute distance matrix, we start at the top right corner, and recursively determine the lowest distance possibility until we reach the starting point. Once this point is reached, the warping path is determined.

Further optimizations Further optimizations to the warping path are possible, as this can be smoothed in order not to include high frequency warps that happen in the presence of high frequency noise.

The resulting path is the resulting output from the implemented function, and is used to warp the target signal into the source signal.

5.4.5 Dynamic time warping applied to average artifact subtraction

The approach taken on this thesis for the removal of the Ballistocardiogram is an enhanced version of the AAS, where the averaging and subtraction steps are refined. A diagram illustrating the basic flow of the refined algorithm is presented in figure 5.7. Each epoch is zero mean and warped into the template. A buffer containing the last n epochs is then used to average the actual template. This template, which contains the artifact waveshape, is subtracted from the next epoch. However, before subtraction it is warped into the next epoch.

5.5 Data

The algorithms were tested both on real EEG data acquired in an fMRI environment, and on simulated data. The EEG acquisition was performed on one healthy and two epileptic subjects (Figure 5.8). The EEG / fMRI consisted in 5 minutes of continuous acquisition in a 1.5T GE CVi/NVi scanner. The EEG was recorded at 1000 Hz through a set of AgCl electrodes connected to an amplifier located outside the scanner room through carbon fiber wires (MagLink, Neuroscan,El Paso, TX, U.S.A.).

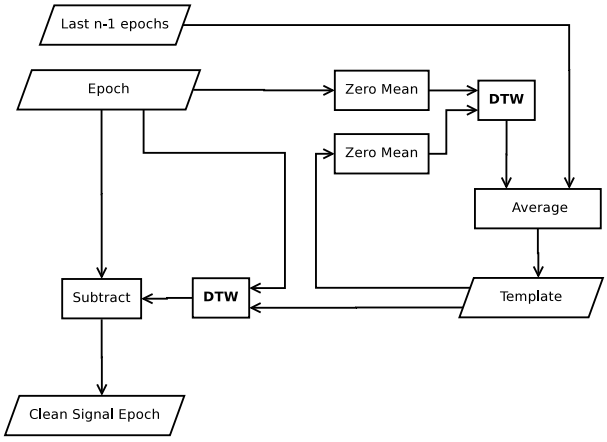

Figure 5.7: The basic workflow of our approach. Each epoch is warped to match the template, and is averaged with the n last epochs. Prior to subtracting the template from the signal, it is warped back into the epoch

Figure 5.8: A subject inside the scanner with the EEG cap

The fMRI sequences acquisition consisted of blocks of 100 brain volumes each one made of 16 EPI images (in plane resolution 3.75 mm and slice thickness of 7 mm, no spacing; echo time 50 s; flip angle of 90°) obtained with a TR = 3 s, corresponding to periods of 5 min of continuous and simultaneous monitoring. The data acquisitions were performed in four different occasions, each time on a different subjects, P1..P3. The patient identified as P1 was healthy, while P2 and P3 suffered from epilepsy. The available channels differed on each patient, and are illustrated on figure 5.9. For each acquired channel, the gradient artifact was filtered by the method proposed by Allen et. al[2], and the BCG was reduced using a simple AAS and our proposed DTW method.

In the simulated data, our goal was to get a close approach to the physiological signal with the Ballistocardiogram artifact and manipulate its characteristics to study the algorithm tolerance and performance to its change. The signal was simulated based on a random signal with a linear distribution. It was low pass filtered simulating a signal with a range of frequencies from 0 to $70Hz$. The artifact was simulated by a *sinc* function ranging from -π to π. The standard length of the artifact was set to 1000 samples, in order to simulate a typical ECG R to R wave distance acquired at a sampling frequency of $1kHz$. To induce artifact timing variations, an *artifact maximum variation* index ranged from 0.5% to 15%, with a linear distribution around the mean value. The amplitude of the artifact was set to twice the absolute mean value of the signal. For each maximum variation, a total of 1000 epochs were generated, each with 1000+-variation samples was generated.

5.6 Results

For the validation of the results we compared our algorithm with AAS as proposed by Allen [2]. Our goal is to compare the performance of our proposed method vs the most commonly used[2]. To achieve this goal both the simulated data and the acquired EEG were tested. In the simulated data, the resulting signals were compared with the original prior to *contamination* and on the acquired data, an autocorrelation analysis[35], frequency spectrum analysis and the template adaptation to the signal were tested.

5.6.1 Simulation

In order to test the results from the simulation, we compared each reduced artifact, by comparing every original epoch (prior to adding the artifact) to the epoch after artifact removal. An illustration of the resulting signals is presented on figure 5.10.

To quantify this result, each epoch from the resulting signals after artifact removal was compared with the original signal before the *sinc artifact* was added. In the presence of a

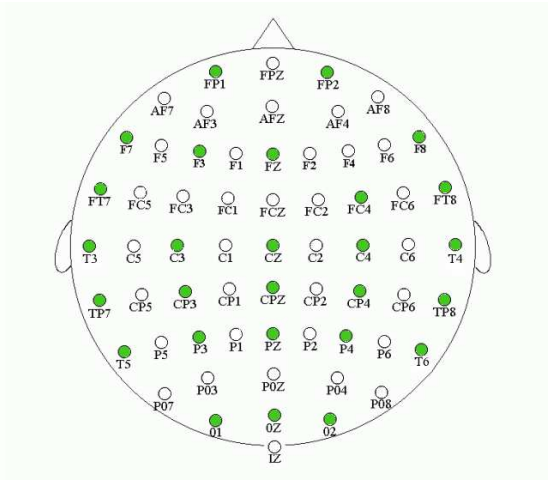

(a) P1

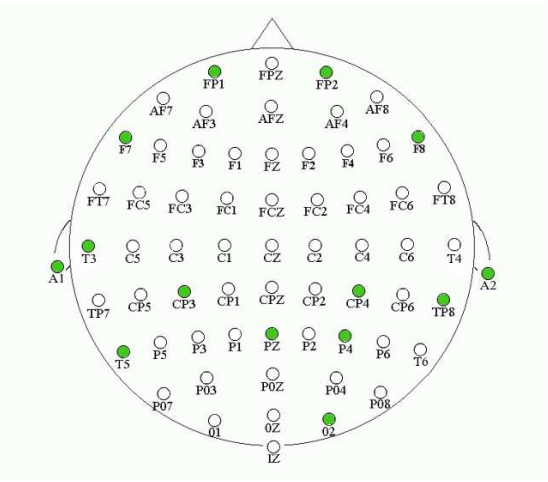

(b) P2

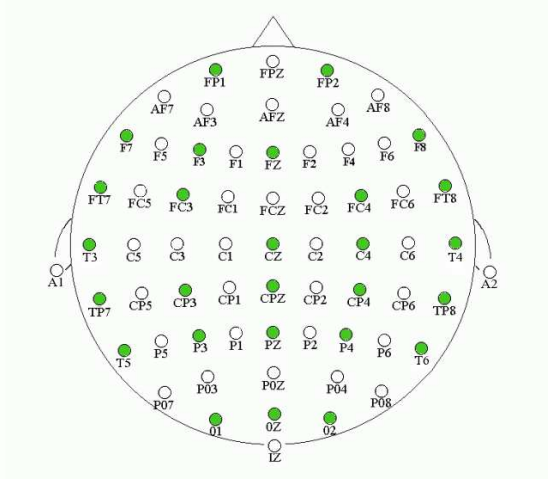

(c) P3

Figure 5.9: The available channels for each patient

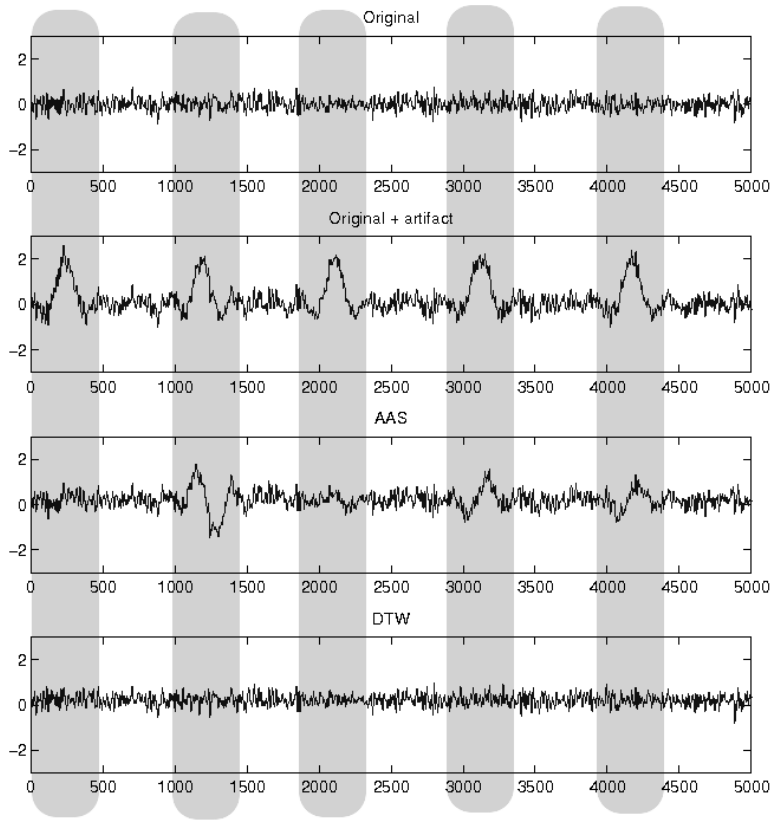

Figure 5.10: A sample signal resulting from the simulation (+-5% artifact warping variation) presenting the original simulated signal, followed by the signal with the added artifact*(sinc* function), the signal after application of the AAS algorithm and the signal after application of our DTW approach. The portions of the signal corresponding to the artifact highest amplitude peaks are highlighted.

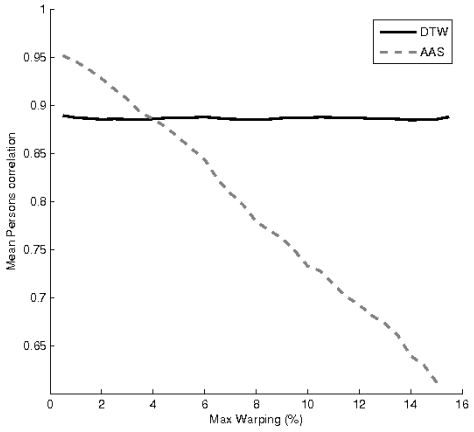

Mean Correlation Values (Simulation) N=1000				
.	DTW		AAS	
variation range(%)	Correlation	σ	Correlation	σ
0.5	0.8843	0.0931	0.9474	0.1019
1.0	0.8876	0.0962	0.9377	0.1037
1.5	0.8852	0.0943	0.9320	0.1011
2.0	0.8850	0.0999	0.9182	0.1075
2.5	0.8843	0.1037	0.9035	0.1128
3.0	0.8871	0.0996	0.8924	0.1098
3.5	0.8855	0.0967	0.8866	0.1105
4.0	0.8833	0.1003	0.8612	0.1173
4.5	0.8887	0.0921	0.8855	0.1064
5.0	0.8892	0.0898	0.8608	0.1097
5.5	0.8891	0.0922	0.8369	0.1214
6.0	0.8857	0.0966	0.8288	0.1223
6.5	0.8870	0.1005	0.8074	0.1321
7.0	0.8823	0.0983	0.7823	0.1384
7.5	0.8843	0.0975	0.7876	0.1403
8.0	0.8868	0.0972	0.7757	0.1419
8.5	0.8843	0.1027	0.7433	0.1483
9.0	0.8900	0.0914	0.7616	0.1385
9.5	0.8876	0.0915	0.7412	0.1409
10.0	0.8870	0.0987	0.7225	0.1469
10.5	0.8860	0.0952	0.6950	0.1453
11.0	0.8876	0.0934	0.7179	0.1440
11.5	0.8879	0.0903	0.6954	0.1435
12.0	0.8872	0.0991	0.6743	0.1537
12.5	0.8859	0.0941	0.6807	0.1437
13.0	0.8814	0.1021	0.6380	0.1458
13.5	0.8877	0.0894	0.6763	0.1368
14.0	0.8863	0.0972	0.6362	0.1395
14.5	0.8820	0.1089	0.5658	0.1483
15.0	0.8879	0.0987	0.6350	0.1410

Table 5.1: The mean signal correlation (N=1000 artifact epochs of 1000 samples each) between the original signal (prior adding the artifact) and the signal after application of each algorithm (AAS and DTW). The left figure illustrates the values on the table (right). The DTW approach shows higher correlation value than the AAS when the time warping variation exceeds 3.5%

perfect removal algorithm, these signals would be identical. The similarity between these signals was computed using the Pearsons Correlation for each epoch. In order to study the efficiency of both algorithms with different warping values, the simulation was repeated for warping variations between 0.5% and 15%.

The resulting mean correlations are summarized and illustrated in table 5.6.1. Although for small artifact warping values (<3.5%) the AAS presents a higher mean correlation value between the original signal and the signal after artifact removal, this decreases as the warping increases. These results suggest a more efficient artifact removal by the DTW approach when the timing artifact varies over 3.5% of the artifact mean length. For smaller variations (<3.5%), the AAS presents better adaptation, since it does not dynamically adapt to the artifact. Since this adaptation can result in template warping to the underlying signal, these

can result in small signal distortion. For a basal ECG rhythm of 80bpm, a variation of just 3bpm or more in the rhythm will degrade the AAS performance in the Ballistocardiogram removal. Simple stimulation can induce this type of variation (such as emotional responses or hypopnea)[20] and, in such situations, the use of DTW will enhance the results.

5.6.2 Acquired EEG

Autocorrelation analysis

The autocorrelation was performed for every channel in each signal, 10s after each minute, for a total of 5 minutes. The computed correlation was the Pearsons Correlation with itself shifted from -3s to 3s (+-3000 samples). As expected when there is no shifting, the correlation value of a signal with itself results in 1. By analysing the values of correlation at different shifts, we can verify the signals periodicity at the values where correlation presents its peaks. Through this analysis all the signals periodic components can be easily identified and the noisy channels are clearly pointed out. Figure 5.2 presents 4 channels autocorrelation graphs for the 3 subjects. The presented graphs show the signal correlation before and after the application of the AAS algorithm and our DTW. On the presented common channels for the 3 subjects, P1 shows a clear acquired signal where both physiological and Ballistocardiogram components can be observed. Both methods successfully reduce the pulse component, although for the DTW approach the remaining components amplitude is preserved, suggesting a lower underlying signal distortion. Subject P2 on channels CP3 and T5 a periodic component can be observed, although the physiological component is missing. This can be due bad contact between the electrode and the scalp. Still, it can be observed that this component is successfully removed by both algorithms. The P3 subjects acquired EEG on channel CP3 shows a small amplitude periodic component. Because of the noise present in this channel, prior to the auto-correlated signal portion on this signal, a good template could not be achieved by neither algorithm, so this periodic component was not removed. Channel CP4, although the physiological components were totally obscured by noise, a periodic component can still be observed, which is reduced by both algorithms. Channel O2 for subject P3 did not contain any physiological signal, probably because of a disconnected electrode. Appendix A contains the detailed autocorrelation graphs from all three subjects.

Template adjustment analysis

In order to analyse the template adaptation to the underlying wave, the Pearsons Correlation was calculated for each epoch (around 1000 samples) along every channel with the template at the epochs position. The values were calculated for the full available EEG time (50s, 50000

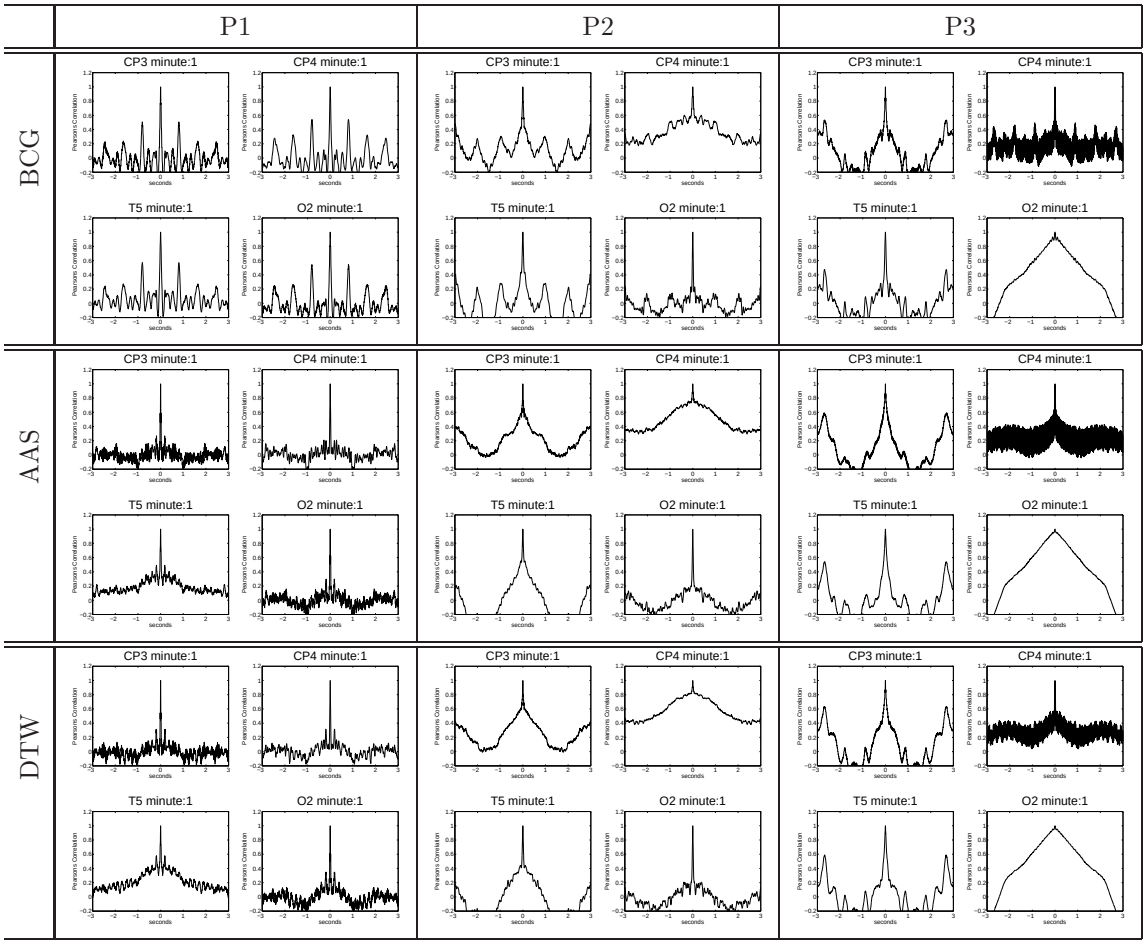

Table 5.2: Autocorrelation graphs from the three subjects P1, P2 and P3.

samples), and the results were averaged for each channel, and subsequently for each patient. This results provide use with a measure of the effectiveness of the template adaptation to each epoch. A better adapted template should better reduce the artifact while minimizing the distortion to the actual underlying physiological EEG. As can be observed in table 5.3, the DTW approach consistently presents higher values of correlation. Appendix B, presents the detailed results obtained for every channel.

Template adaptation mean values (N=50)				
–	DTW		AAS	
Subject	Correlation Coefficient	σ	Correlation Coefficient	σ
P1	0.61	0.17	0.55	0.16
P2	0.60	0.13	0.46	0.14
P3	0.54	0.14	0.40	0.15

Table 5.3: Mean Pearsons correlation values for the tested patients (N=50 epochs each with 800-1100 samples)

Frequency spectrum analysis

The frequency spectrum was obtained for each subject and the results were averaged in order to compare our proposed algorithm with the standard average artifact subtraction. The averaged frequency plots are presented in figure 5.11. We can observe that both algorithms successfully remove the frequency components usually associated with the BCG however, the DTW algorithm presents a slightly greater reduction on the 4-12Hz band. Due to small pulse variations present in the acquired signals and a lack of an EEG signal acquired for each subject under similar conditions outside the scanner, which would provide a standard spectrum, conclusive results cannot be taken from this data.

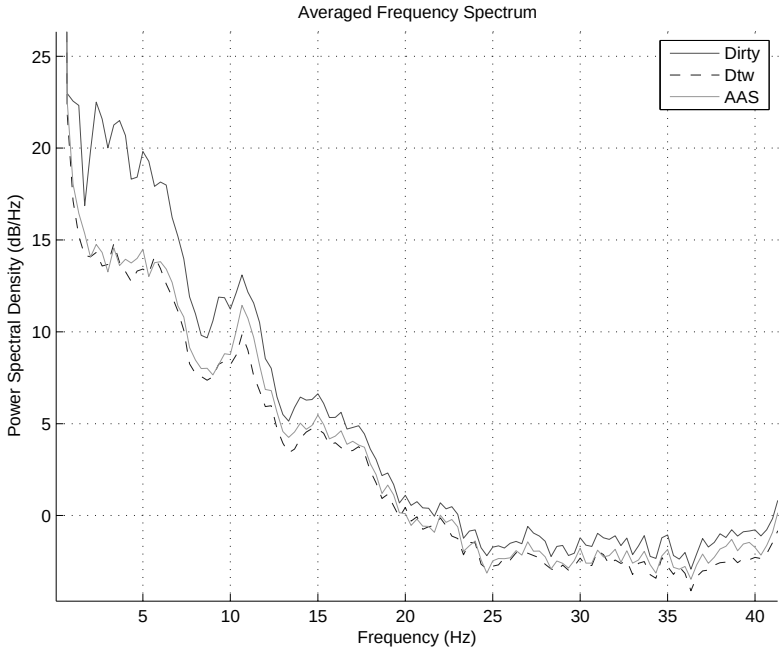

Figure 5.11: The averaged frequency spectra using the Welch method for the tested subjects before and after the application of our proposed algorithm (DTW) and the most commonly used(AAS)

Chapter 6

Discussion

The main goal in artifact removal methods is always the removal of the artifact while minimizing the distortions on the underlying signal. The most popular methods proposed for the BCG artifact removal, although providing an acceptable signal, and because of the simplicity of their implementation, are becoming a standard for the BCG removal but have been criticized because of the principle of its initial assumptions[35]. By assuming a periodicity in an artifact with a physiological source, we always end up distorting the underlying signal to a certain degree. Our goal is to provide an algorithm that shares the AAS principles, but overcomes the problems resulting from its initial assumptions. Our proposed algorithm is, contrary to the simple AAS, able to dynamically adapt the template time axis to each signal epoch between two successive R ECG waves. The assumption that the best artifact alignment is the one resulting from the application of the lowest cost function, is acceptable as long as the artifact is larger in amplitude than the underlying physiological signal. The possible drawback of our proposed method is that by dynamically time warping the signal with a minimum cost function, we could be distorting the signal to some degree. Our simulation results for different levels of signal variation show that our algorithm becomes more efficient in the artifact removal when signal warping was present, with a linear distribution over 3.5% the epoch length. This result shows the potential for the application of the algorithm when in presence of an unstable or varying pulse, and consequent artifact variation. Although physiological EEG data used for the analysis on this thesis did not predict inducing pulse variations and the subjects did not present significant pulse rate variability, the measured template adaptation was consistently superior with our method, suggesting that the BCG, even with a stable pulse, presents sufficient variation for our method to outperform the most commonly used in the literature (AAS). Another good potential indicator is the increase in the effectiveness of the artifact adaptation with the increase of the artifact / signal ratio. Since for higher magnetic field strengths the amplitude of the BCG also increases, the pro-

posed algorithm should further improve the quality of the template adaptation and therefore improve the BCG reduction. A drawback for the DTW approach is the greater complexity of the algorithm and consequently the higher demand for more processing power. This can somehow limit its application when real time acquisition is needed. An implementation of the algorithm in a compiled programming language could speed up the processing as our approach was implemented in an interpreted language (MATLAB), much slower than a compiled solution. This compromise between the artifact variation, desired removal quality and processing speed should be taken in account when applying the algorithm.

Chapter 7

Conclusions and future work

The work covered on this thesis provides a state of the art insight into different artifact removal, mainly in techniques based on average artifact subtraction. Its limitations have been explored and a solution to overcome them has been proposed. The proposed algorithm has been tested under simulated conditions where it presented its potential for the application of physiological EEG acquired inside the scanner. These were performed on the available data that although did not present the desired heart rate variability, demonstrated a better adaptation of the template to each artifact. The next step for a better understanding of the periodic characteristics of the Ballistocardiogram would be the experiment performed by Nakamura et. al.[35] where the underlying physiological signal is eliminated from the acquired EEG. This data would validate our assumptions in the development of the new dynamic time warping approach, as they were mostly based on the work described by other authors. Also, the EEG acquired on the patient prior entering the magnetic environment is of great value to validate the attenuated frequencies on the BCG contaminated signal. The algorithm should be further explored for different static field strenghts, where its amplitude ratio to the underlying physiological EEG should be higher, thus further improving the template adjustment and consequently the BCG removal with our proposed dynamic time warping approach. We are pleased that the present work was submitted and accepted on the *14-th Nordic - Baltic Conference on Biomedical Engineering and Medical Physics, Riga, Latvia 16-20 June 2008.*

Appendix A

Autocorrelation analysis

This appendix contains the autocorrelation graphs for all the EEG channels of every analysed subject.

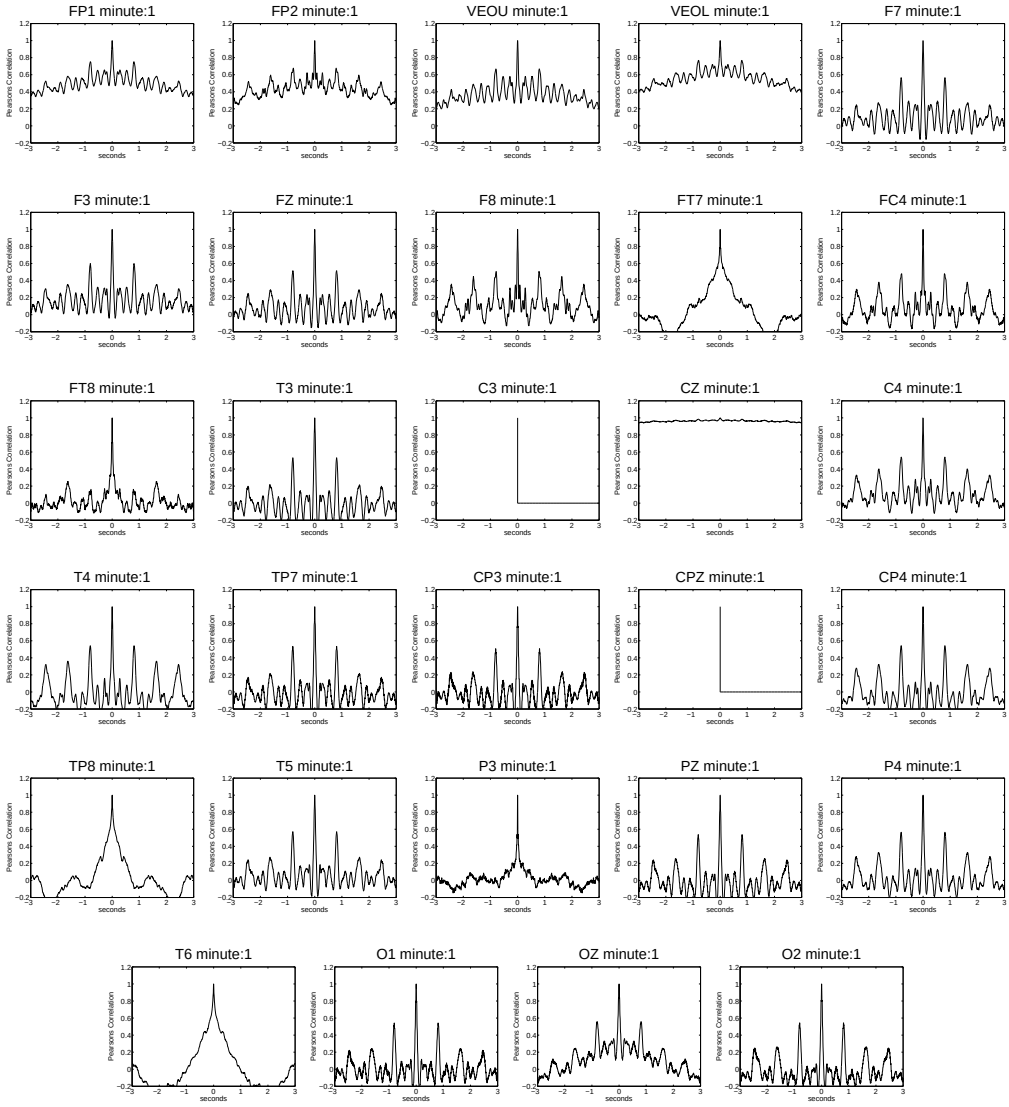

Figure A.1: Autocorrelation graphs for subject P1, with Gradient artifact removed

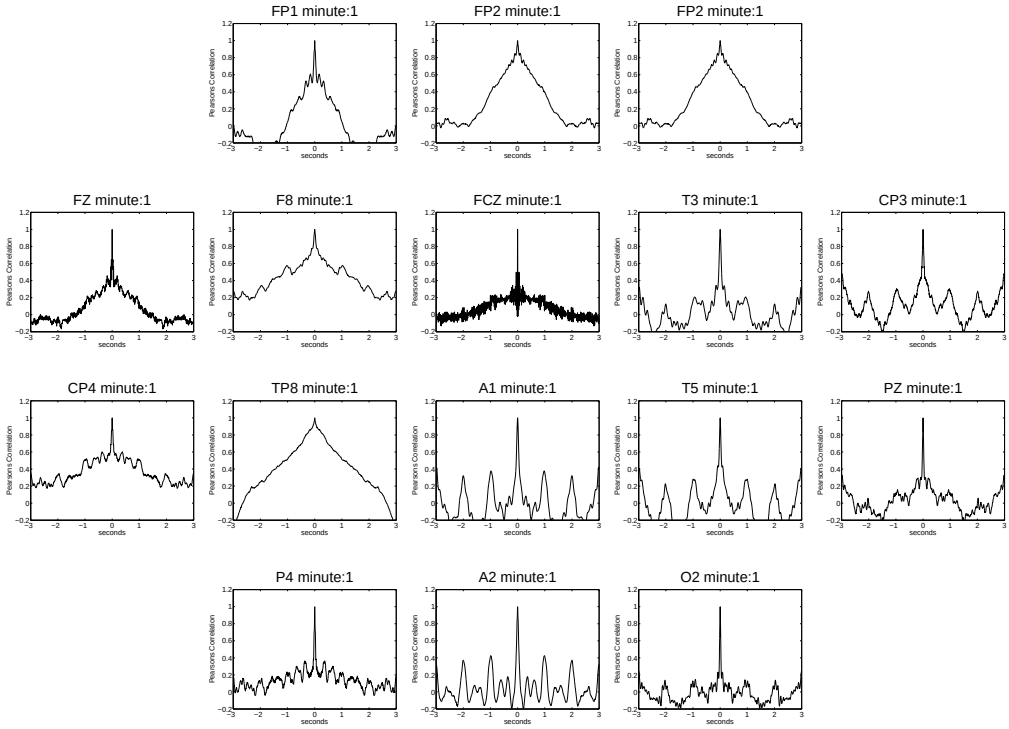

Figure A.2: Autocorrelation graphs for subject P2, with Gradient artifact removed

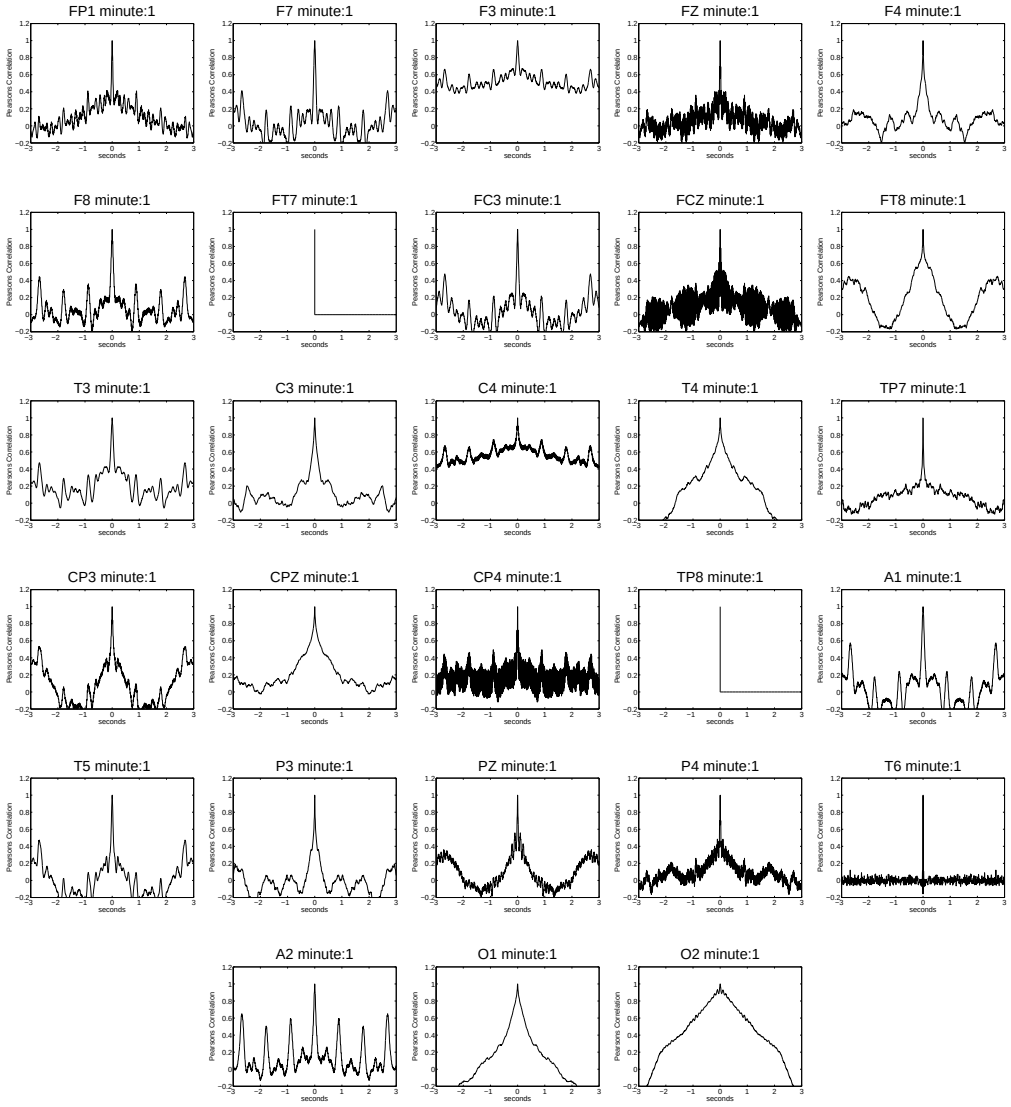

Figure A.3: Autocorrelation graphs for subject P3, with Gradient artifact removed

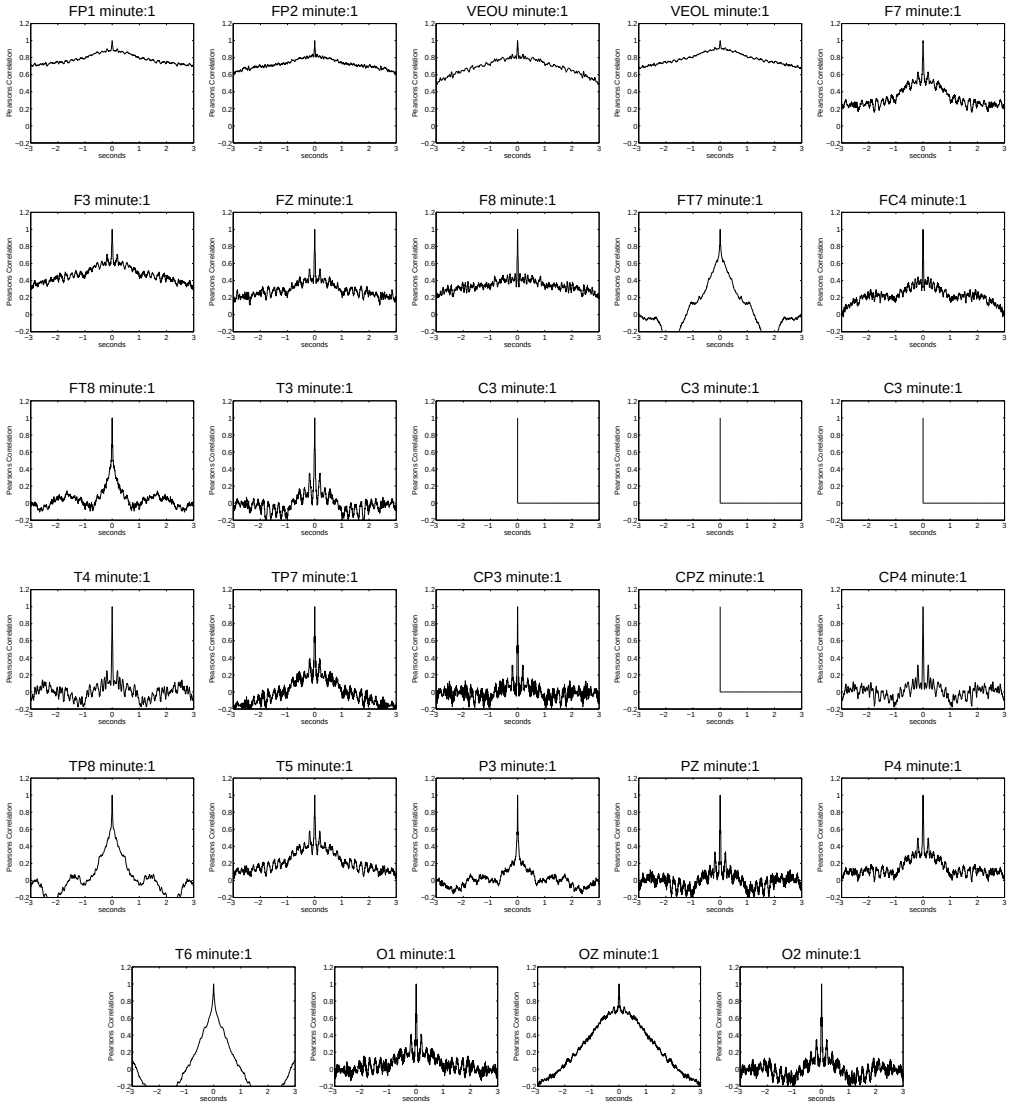

Figure A.4: Autocorrelation graphs for subject P1, with Gradient and BCG removed with the DTW method

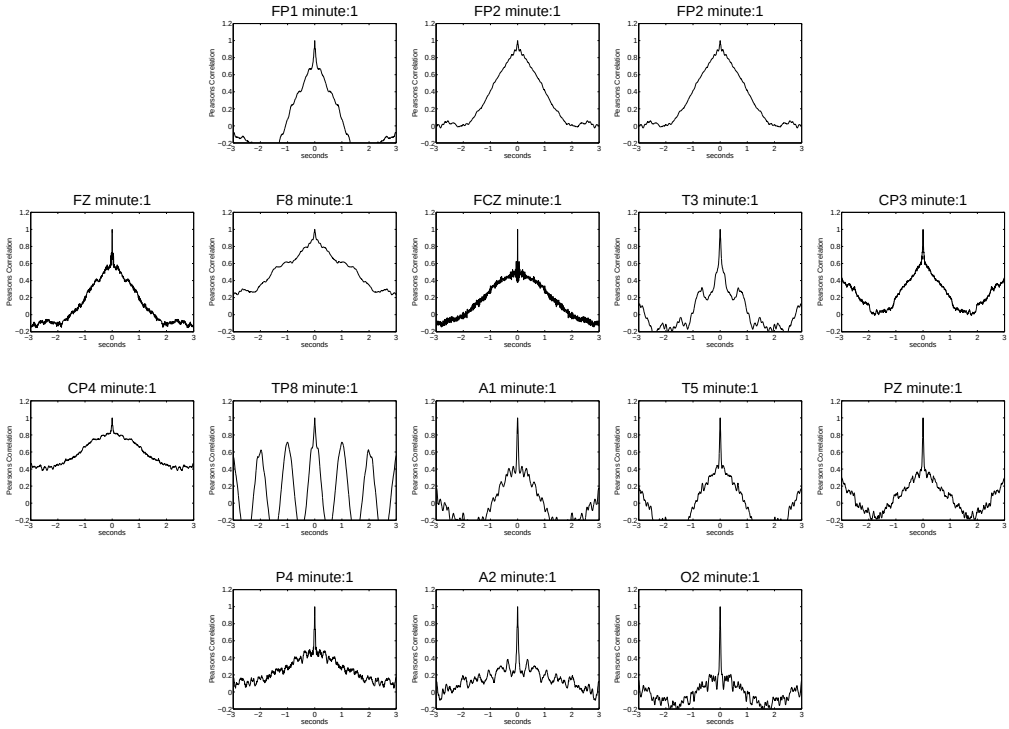

Figure A.5: Autocorrelation graphs for subject P2, with Gradient and BCG removed with the DTW method

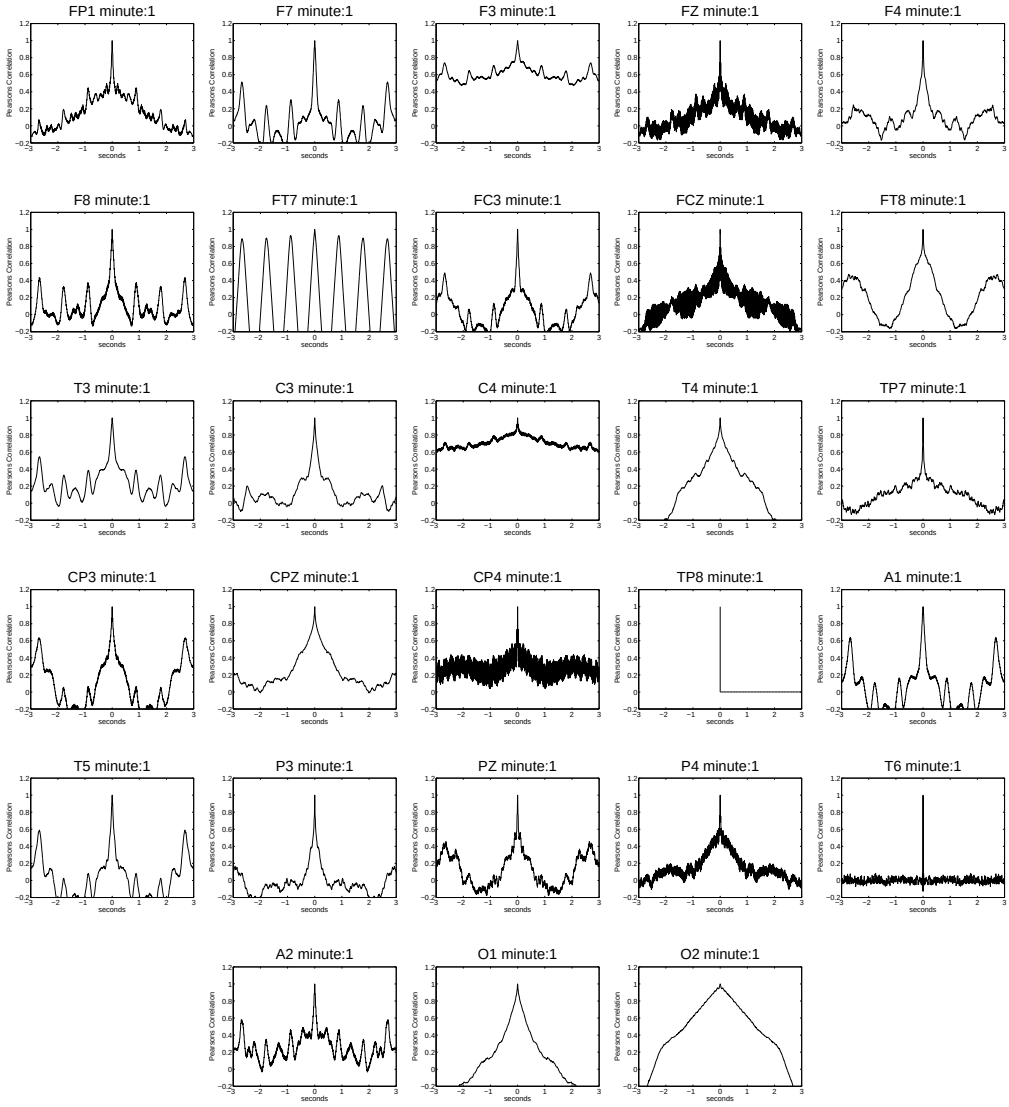

Figure A.6: Autocorrelation graphs for subject P3, with Gradient and BCG removed with the DTW method

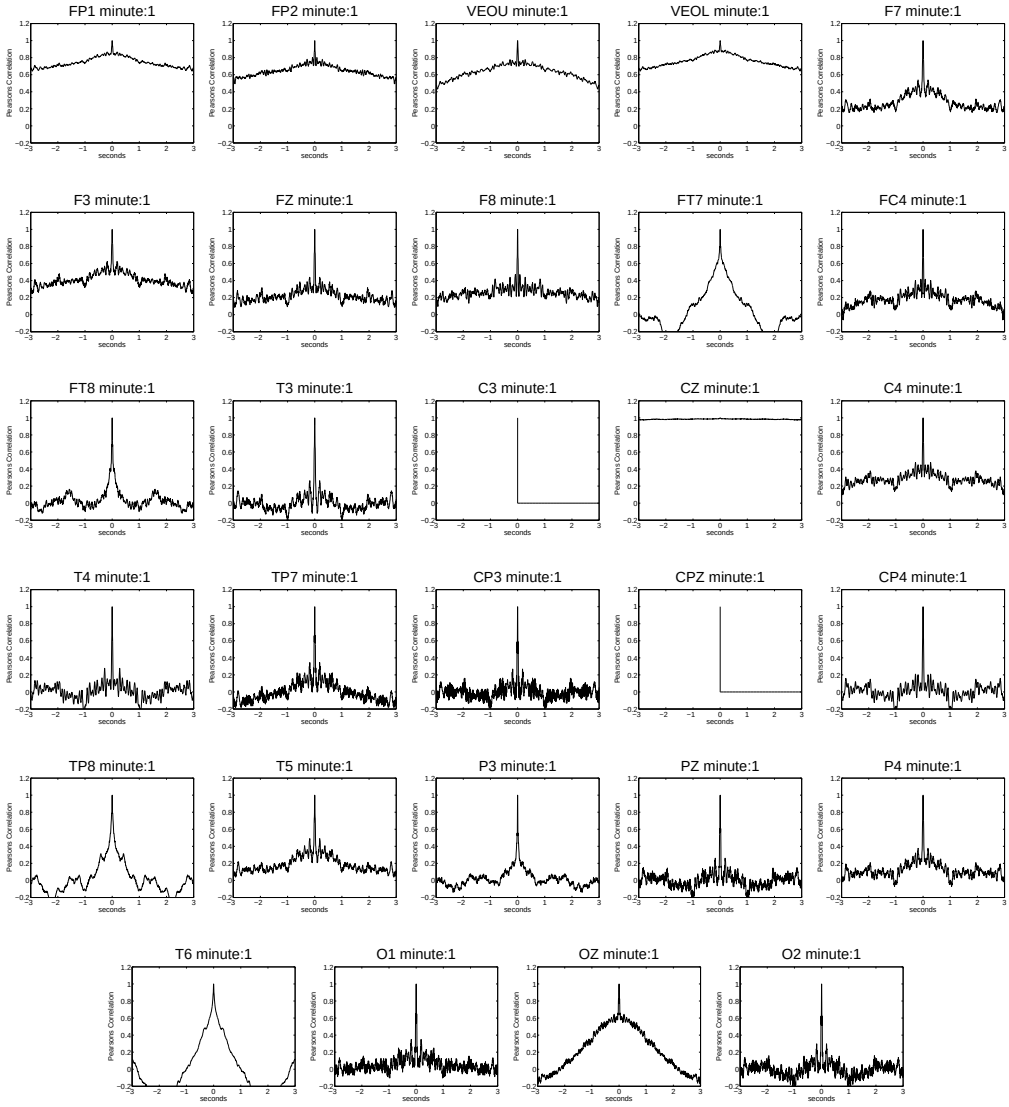

Figure A.7: Autocorrelation graphs for subject P1, with Gradient and BCG removed with the AAS method

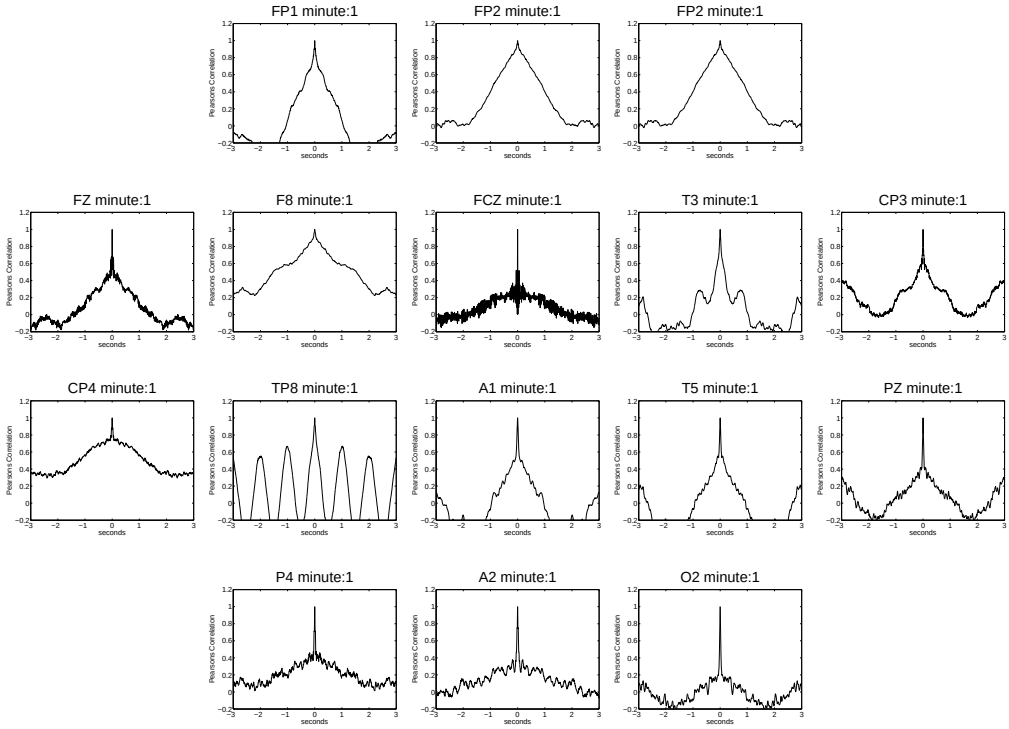

Figure A.8: Autocorrelation graphs for subject P2, with Gradient and BCG removed with the AAS method

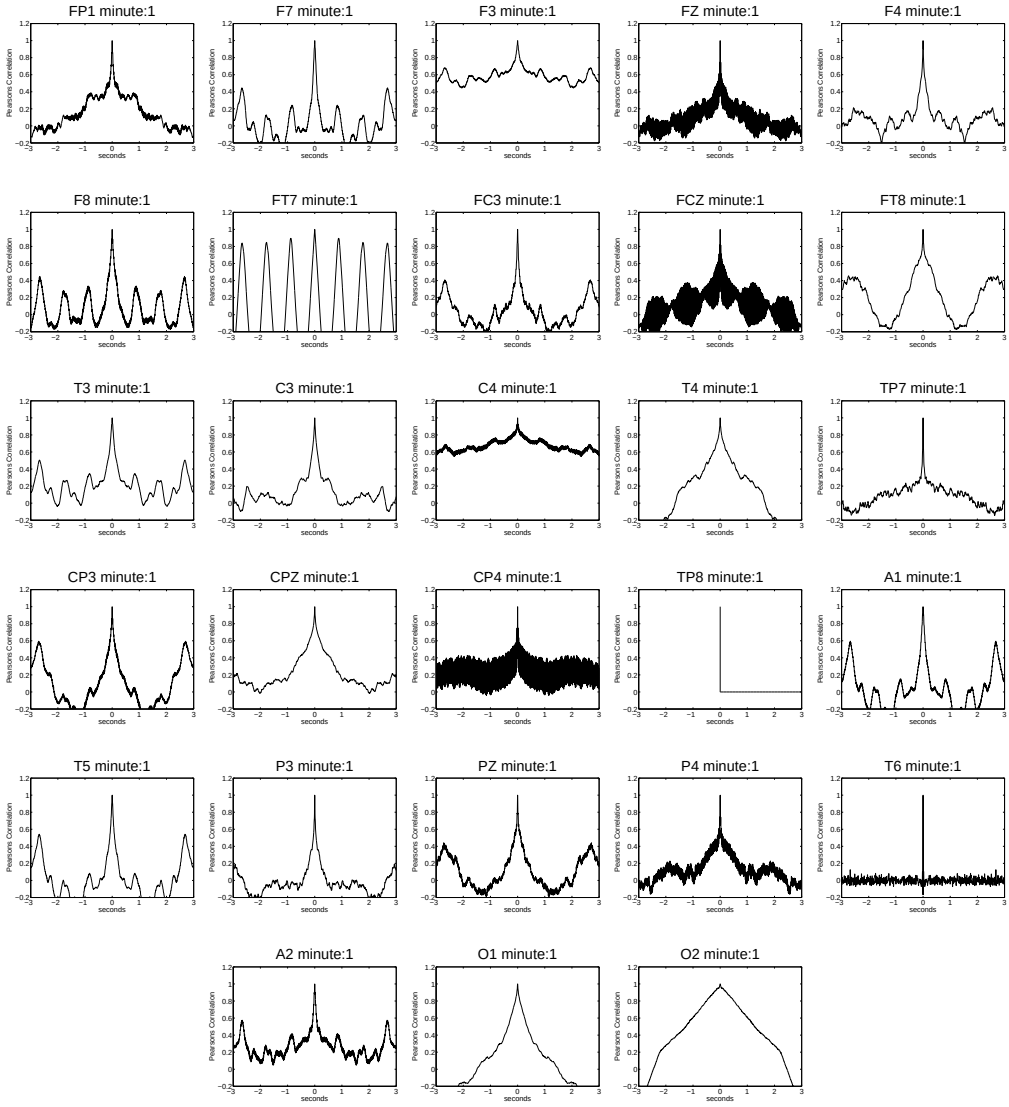

Figure A.9: Autocorrelation graphs for subject P3, with Gradient and BCG removed with the AAS method

Appendix B

Template adaptation analysis

This appendix contains the mean correlation values between the the template and each epoch for every channel acquired for every subject.

Average Correlation Values				
–	DTW		AAS	
Channel	Correlation Coefficient	σ	Correlation Coefficient	σ
EKG1	0.00	0.00	0.00	0.00
EKG2	0.00	0.00	0.00	0.00
FP1	0.84	0.21	0.79	0.20
FP2	0.81	0.21	0.70	0.21
VEOU	0.84	0.22	0.79	0.20
VEOL	0.83	0.19	0.77	0.19
F7	0.85	0.21	0.81	0.20
F3	0.85	0.20	0.80	0.19
FZ	0.85	0.21	0.80	0.20
F4	0.00	0.00	0.00	0.00
F8	0.82	0.20	0.73	0.18
FT7	0.57	0.18	0.43	0.18
FC3	0.00	0.00	0.00	0.00
FCZ	0.00	0.00	0.00	0.00
FC4	0.83	0.20	0.75	0.17
FT8	0.69	0.19	0.57	0.22
T3	0.86	0.19	0.83	0.17
C3	0.49	0.27	0.45	0.29
CZ	0.82	0.19	0.49	0.24
C4	0.84	0.20	0.78	0.19
T4	0.80	0.21	0.75	0.20
TP7	0.85	0.21	0.81	0.17
CP3	0.85	0.20	0.79	0.17
CPZ	0.84	0.18	0.76	0.15
CP4	0.85	0.21	0.81	0.20
TP8	0.45	0.26	0.33	0.30
A1	0.00	0.00	0.00	0.00
T5	0.86	0.19	0.83	0.17
P3	0.46	0.22	0.35	0.28
PZ	0.85	0.21	0.81	0.18
P4	0.85	0.21	0.81	0.19
T6	0.45	0.29	0.37	0.29
A2	0.00	0.00	0.00	0.00
O1	0.85	0.20	0.81	0.16
OZ	0.74	0.26	0.67	0.28
Mean	0.61	0.17	0.55	0.16

Table B.1: Average correlation values for subject P1

Average Correlation Values				
–	DTW		AAS	
Channel	Correlation Coefficient	σ	Correlation Coefficient	σ
EKG1	0.00	0.00	0.00	0.00
EKG2	0.00	0.00	0.00	0.00
FP1	0.66	0.17	0.52	0.17
FP2	0.64	0.20	0.52	0.20
FZ	0.76	0.11	0.47	0.15
F8	0.70	0.17	0.60	0.18
FCZ	0.86	0.08	0.42	0.12
T3	0.72	0.18	0.64	0.16
CZ	0.00	0.00	0.00	0.00
CP3	0.76	0.14	0.55	0.16
CP4	0.80	0.13	0.52	0.14
TP8	0.46	0.31	0.29	0.29
A1	0.80	0.18	0.76	0.16
T5	0.76	0.17	0.68	0.16
PZ	0.70	0.14	0.53	0.15
P4	0.72	0.13	0.56	0.14
A2	0.80	0.17	0.75	0.15
Mean	0.60	0.13	0.46	0.14

Table B.2: Average correlation values for subject P2

Average Correlation Values				
–	DTW		AAS	
Channel	Correlation Coefficient	σ	Correlation Coefficient	σ
EKG1	0.00	0.00	0.00	0.00
EKG2	0.00	0.00	0.00	0.00
FP1	0.82	0.17	0.71	0.14
FP2	0.00	0.00	0.00	0.00
VEOU	0.00	0.00	0.00	0.00
VEOL	0.00	0.00	0.00	0.00
F7	0.79	0.17	0.69	0.16
F3	0.78	0.16	0.65	0.14
FZ	0.81	0.14	0.61	0.12
F4	0.57	0.20	0.36	0.27
F8	0.79	0.17	0.67	0.16
FT7	0.50	0.23	0.29	0.29
FC3	0.75	0.15	0.60	0.15
FCZ	0.80	0.13	0.50	0.13
FC4	0.00	0.00	0.00	0.00
FT8	0.55	0.26	0.33	0.27
T3	0.79	0.17	0.70	0.16
C3	0.53	0.22	0.36	0.28
CZ	0.00	0.00	0.00	0.00
C4	0.81	0.16	0.63	0.16
T4	0.57	0.19	0.35	0.24
TP7	0.60	0.24	0.42	0.20
CP3	0.79	0.16	0.62	0.16
CPZ	0.51	0.28	0.34	0.28
CP4	0.81	0.14	0.58	0.14
TP8	0.53	0.22	0.30	0.26
A1	0.83	0.16	0.75	0.15
T5	0.80	0.18	0.71	0.16
P3	0.51	0.28	0.33	0.28
PZ	0.75	0.16	0.57	0.16
P4	0.75	0.13	0.54	0.14
T6	0.70	0.10	0.40	0.16
A2	0.85	0.16	0.78	0.15
O1	0.53	0.31	0.35	0.28
OZ	0.00	0.00	0.00	0.00
Mean	0.54	0.14	0.40	0.15

Table B.3: Average correlation values for subject P3

Appendix C

Published paper arising from this dissertation

This appendix contains the paper published on the *14-th Nordic - Baltic Conference on Biomedical Engineering and Medical Physics, Riga, Latvia 16-20 June 2008*

EEG-fMRI Ballistocardiogram removal: A new non-linear Dynamic Time Warping approach

J.L. Kustra[1], J.M. Fernandes[1,2] and J.P. Silva Cunha[1,2]

[1] IEETA, University of Aveiro, Aveiro, Portugal
[2] DETI, University of Aveiro, Aveiro, Portugal

Abstract—**Functional Magnetic Resonance Imaging (fMRI) is a promising technique to spatially identify activated areas. However, because of its limited time resolution (about one volume every 3 seconds), integration with a high temporal resolution method (Electroencephalography (EEG)) has shown to be promising. Two main artifacts rise on the EEG in this setup: The imaging artifact and the Ballistocardiogram artifact (BCG). The focus of this paper is to present a new approach for BCG removal. The most common method for its removal is based on average wave shape subtraction. This method assumes a deterministic approach to the BCG, which, as every analog biomedical signal, is not a good assumption. In this paper we present and evaluate, for the first time, a Ballistocardiogram removal adaptive algorithm based on dynamic time warping (DTW)[1]. Although for stable pulse this method can slightly distort the wave shape, we believe it can be reliable to deal with greater BCG time variations, like in the presence of arrhythmia, or during emotion stimulation.**

Keywords— **electroencephalography, functional magnetic resonance imaging, multimodal, ballistocardiogram, dynamic time warping**

I. Introduction

fMRI is a relatively new magnetic resonance imaging (MRI) based technique that allows monitoring of the brain activation patterns by measuring the magnetic variation induced by changes in the blood flow associated to brain neural activity. The neural activity produces an increase in blood flow (with a delay of about 2 seconds) richer in oxyhemoglobin to compensate the increase in oxygen consumption. This change in oxyhemoglobin is called the Blood Oxygen Level Dependent response or BOLD effect [2]. The local fluctuations in BOLD induce magnetic variations that are susceptible to be detected through T2-weighted gradient-echo echo-planar imaging[3]. When BOLD activations and deactivation are time related with specific events, they can be related to metabolic response in the brain. Therefore fMRI provides an indirect way of studying the brain activity[3]. Although it provides a good spatial resolution, the drawback of fMRI is its poor time resolution (typically one head volume acquisition every 3 seconds in a 1.5 T MRI machine), a limiting factor when observing the rapid brain electrical dynamics. However, these can be reliably characterised through the electroencephalography (EEG) where electric potential variations, induced by electrical brain activity, can be measured on the scalp surface in high sampling frequencies (≥200Hz). In contrast to the ability of capturing events in real time, EEG has a limited spatial resolution. Integrating both techniques (EEG-fMRI) represents an added value both in normal and abnormal brain activity characterisation[4]. This integration is not free from problems due to artifacts induced in EEG by magnetic field variations: EEG relies on cables connected to the subjects head to capture the electric potential over the scalp that, when acquired inside a MRI shielded room, are subjected to electric inductance generated by the very strong static and varying magnetic fields in fMRI sequences, obscuring the original EEG signal. In this environment the two most relevant artifacts are: the imaging artifact originated by magnetic field gradient fast alterations and the Ballistocardiogram (BCG) induced by heart pulse[4]. The removal of the BCG artifacts is the focus of the present work, where we present a new approach to address this problem. The BCG artifact occurs between two successive Electrocardiogram (ECG) R waves, and so it is associated with the subjects pulse. The pointed causes for its occurrence have been the subjects head motion, the expansion and contraction of the scalp arteries in the static magnetic field and the Hall effect when hemoglobin flows perpendicular to the static field[5-7]. This last source is believed to be very small, because of the approximate equal number of positive and negative ions in the circulation, and the random blood vessel distribution, that leads to a cancellation of the induced signals [8, 9]. Since this artifact obscures the underlying physiological EEG, methods for its removal have been proposed. The proposed methods rely on different techniques such as average artifact subtraction(AAS), Adaptive Filtering and independent component analysis(ICA)[10, 11]. Bonmassar *et al*[8] proposes a method to remove the BCG artifact based on the principle that the most significant contributions to the artifact are due to small movements in the scanner. By using a motion sensor in a target position on the subjects scalp, these are quantified, an adaptive noise cancellation algorithm was used and the system was modeled as a linear combination of the physiological contributions with the

induced artifact, similarly to the above explained methods. These artifact components are calculated based on the motion sensor output, producing a Finite Impulse Response (FIR) filter kernel which is used to estimate the noise signal that is subtracted from the acquired EEG. Although this method presented good results its setup is not trivial as it requires a motion sensor. The most widely used method for BCG removal is the one proposed by Allen et al.[5]. It relies on estimating the artifact wave shape by averaging several artifacts, followed by the subtraction of the averaged artifact template to each position. It is capable of successfully removing the artifact, as long as the artifact is assumed stable from frame to frame. However, the BCG results from the subjects physiological responses and to assume this signal is deterministic seems like an unrealistic approach[11]. An enhanced version of this algorithm is presented by Sijbers *et al*[7] where, prior to template averaging, time scaling of the artifacts to a fixed time interval is performed. Each artifact is then normalized with respect to mean and standard deviation. Also, it is subjected to a wavelet filter where the wavelet coefficients of the highest frequencies are set to zero. Although a variation in the artifact is assumed, it is still deterministic because it results from a linear wave shape variation, proportional to the R-R distance. This leaves no room for spontaneous wave shape warps, very common in physiological signals in many situations such as reaction to motor of visual stimulation. The approach taken in this paper is based on average artifact subtraction, and it is capable of adapting itself to each artifact epoch by applying Dynamic Time Warping (DTW)[1] prior to averaging the template and warping the template back before subtraction.

II. Materials and methods

A. Data

The algorithms were tested both on real EEG data acquired in an fMRI environment, and on simulated data. The EEG acquisition was performed on one healthy and two epileptic subjects. The EEG/fMRI consisted in 5 minutes of continuous acquisition in a 1.5T GE CVi/NVi scanner. The EEG was recorded at 1000 Hz through a set of AgCl electrodes connected to an amplifier located outside the scanner room through carbon fiber wires (MagLink, Neuroscan, El Paso, TX, U.S.A.). The data acquisitions were performed in three different occasions, each time on a different subjects, P1..P3. The patient identified as P1 was healthy, while P2 and P3 suffered from epilepsy. For each acquired channel, the gradient artifact was filtered by the method proposed by Allen *et al*[5], and the BCG was reduced using a simple AAS and our proposed DTW method. In the simulated data, our goal was to get a close approach to the physiological signal with the Ballistocardiogram artifact and manipulate its characteristics to study the algorithm tolerance and performance to its change. The signal was simulated based on a random signal with a linear distribution. It was low pass filtered simulating a signal with a range of frequencies from 0 to 70Hz. The artifact was simulated by a *sinc* function ranging from $-\pi$ to π. The standard length of the artifact was set to 1000 samples, in order to simulate a typical ECG R to R wave distance acquired at a sampling frequency of 1 kHz. To induce artifact timing variations, we generated an *artifact maximum variation* index ranged from 0.5% to 15%, with a linear distribution around the mean value. The amplitude of the artifact was set to twice the absolute mean value of the signal. For each maximum variation, a total of 1000 epochs were generated.

B. Dynamic time warping

Dynamic Time Warping (DTW) is a technique for aligning two time series in order to find a dissimilarity measure using nonlinear temporal alignment. This algorithm has found its application in the solution of different problems such as handwriting recognition or speech recognition. Its use in the analysis of electrophysiological signals has been of great importance in the analysis of spike patterns, event related potentials and in the analysis of the ECG waveform. It provides the ability to compare two time series because it provides an index of the similarity of two time series. In order to calculate this index, the target time series is nonlinearly warped into the other, stretching and compressing along the X axis, providing a minimum cost alignment between two time series. The details of its implementation can be found in Keogh *et al*[1]. In this paper we present DTW as potential tool to improve the removal of the BCG by not blindly averaging to the template and subtracting it from the signal, but prior to those operations, dynamically warping the signals.

C. Applying DTW to the average artifact subtraction

To deal with these variations, the template must dynamically adapt to every epoch. To solve this problem, the previously described DTW algorithm can be used. Therefore, before averaging each epoch, this is dynamically warped to the current template, obtaining the lowest cost alignment between the two signals. By adding this step, we avoid one portion of the signal averaging with *the wrong* part of the signal. The template achieved by this method is used, just like in AAS, to be subtracted to the signal at defined posi-

tions. However, prior to subtraction, the template, is warped to match the current signal position.

III. Results

For the validation of the results we compared our algorithm with AAS as proposed by Allen[5], which is the most commonly used approach. In the simulated data, we compared each reduced artifact, by calculating a correlation index for every original epoch (prior to adding the artifact) to the epoch after artifact removal with AAS and our DTW approach. An illustration of the resulting signals is presented on Fig. 1. In the presence of a perfect removal algorithm, the original and resulting signal after the algorithm application would be identical. In order to study the efficiency of both algorithms with different warping values, the simulation was repeated for warping variations between 0.5% and 15%. The resulting mean correlations are illustrated in Fig.2. Although for small artifact warping values (<3.5%) the AAS presents a higher mean correlation value between the original signal and the signal after artifact removal, this decreases as the warping increases. For the acquired data, we compared the template adaptation to each epoch. A better adapted template should better reduce the artifact while minimizing the distortion to the actual underlying physiological EEG. The Pearsons Correlation was calculated for each epoch (of 1000 samples) along every channel with the template at the epochs position. The values were calculated for the full available EEG time (50s, 50000 samples), and the results were averaged for each channel, and subsequently for each patient. As can be observed in Table 1, the DTW approach consistently presents higher values of correlation.

Table 1 Mean Correlation Values (EEG)

	DTW		AAS	
Subject	Correlation	σ	Correlation	σ
P1	0.61	0.17	0.55	0.16
P2	0.60	0.13	0.46	0.14
P3	0.54	0.14	0.40	0.15

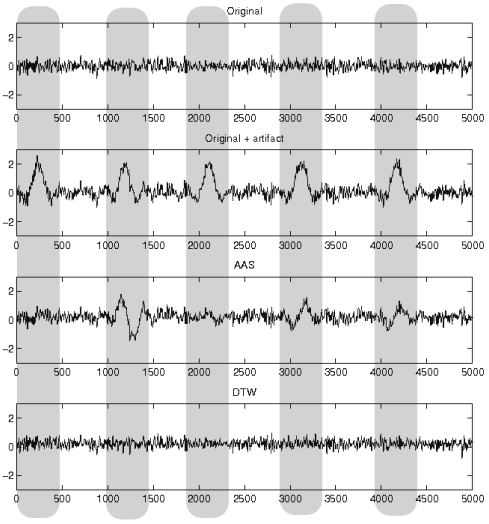

Fig. 1 A signal resulting from the simulation presenting the original simulated signal (5000 samples), followed by the signal with the added artifact (*sinc* function) with +-5% artifact warping variation, the signal after application of the AAS algorithm and the signal after application of our DTW approach. The portions of the signal corresponding to the artifact highest amplitude peaks are highlighted

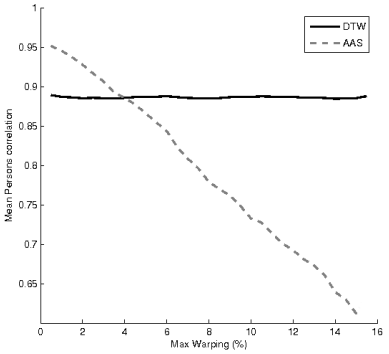

Fig. 2 The mean signal correlation (N=1000 artifact epochs of 1000 samples each) between the original signal (prior adding the artifact) and the signal after application of each algorithm (AAS and DTW). The DTW approach shows higher correlation value than the AAS when the time warping variation exceeds 3.5%

IV. Discussion

The main goal in artifact removal methods is always the removal of the artifact while minimizing the distortions on the underlying signal. The most popular methods proposed for the BCG artifact removal, although providing an acceptable signal for some situations, and because of the simplicity of their implementation, are becoming a standard for the BCG removal but have been criticized because of the principle of its initial assumptions[11]. By assuming a periodicity in an artifact with a physiological source, we always end up distorting the underlying signal to a certain degree. Our goal is to provide an algorithm that shares the AAS principles, but overcomes the problems resulting from its initial assumptions. The proposed algorithm is, contrary to the simple AAS, able to dynamically adapt the template time axis to

each signal epoch between two successive R ECG waves. The assumption that the best artifact alignment is the one resulting from the application of the lowest cost function is acceptable as long as the artifact is larger in amplitude than the underlying physiological signal. The possible drawback of our proposed method is that by dynamically time warping the signal with a minimum cost function, we could be distorting the signal to some degree. Our simulation results for different levels of signal variation show that our algorithm becomes more efficient in the artifact removal when signal warping was present, with a linear distribution over 3.5% the epoch length. For a basal ECG rhythm of 80bpm, a variation of just 3bpm or more in the rhythm will degrade the AAS performance in the BCG removal. Stimulation can induce this type of variation (emotional responses or hypopnea)[12]. In such situations, the use of DTW will enhance the results. For the real EEG data our DTW method was consistently superior by presenting better correlation values, suggesting that it is better for the BCG removal, even with small and spontaneous pulse variations. Since the adaptation improves with the increase of the artifact/signal ratio and for higher magnetic field strengths the amplitude of the BCG increases, our algorithm should further improve the quality of the template adaptation and further improve the BCG reduction in EEG-fMRI data from 3T or higher MRI machines. Because of the greater complexity of the algorithm and consequently a higher demand for processing power, a compromise between the artifact variation, desired removal quality and processing speed should be taken in account when applying the algorithm.

V. Conclusions

The DTW approach for the removal of the BCG shows a very good potential to overcome the AAS limitations. More work is needed for the algorithm to be further explored with different static field strenghts, where its amplitude ratio to the underlying physiological EEG should be higher, improving the template adjustment and consequently the BCG removal.

Acknowledgment

We would like to thank the EpilBi project (POSC/EEA-CPS/60977/2004) and its funding institution, FCT (Portuguese Science and Technology Agency), IEETA (www.ieeta.pt), Alberto Leal, M.D. and Nicolas Lori for their contributions to the current work.

References

1. Keogh, E. and M. Pazzani, *Derivative Dynamic Time Warping*. 2001.
2. Oswaga, S., et al., Brain magnetic resonance imaging with contrast dependent on blood oxygenation, in Proceedings of the National Academy of Sciences. 1990. p. 9868--9872.
3. Cohen, M.S. and R.M. DuBois, Stability, repeatability, and the expression of signal magnitude in functional magnetic resonance imaging, in Journal of Magnetic Resonance Imaging. 1999. p. 33--40.
4. Salek-Haddadi, A., et al., EEG quality during simultaneous functional MRI of interictal epileptiform discharges, in Magn Reson Imaging. 2003. p. 1159--1166.
5. Allen, P.J., et al., Identification of EEG Events in the MR Scanner: The Problem of Pulse Artifact and a Method for Its Subtraction, in NeuroImage. 1998. p. 229--239.
6. Hill, R.A., et al., Hemodynamic and metabolic aspects of photosensitive epilepsy revealed by functional magnetic resonance imaging and magnetic resonance spectroscopy, in Epilepsia. 1999. p. 912--920.
7. Sijbers, J., et al., Reduction of ECG and gradient related artifacts in simultaneously recorded human EEG/MRI data, in Magnetic Resonance Imaging. 2000. p. 881--886.
8. Bonmassar, G., et al., Motion and ballistocardiogram artifact removal for interleaved recording of EEG and EPs during MRI, in Neuroimage. 2002. p. 1127--1141.
9. Schomer, D.L., et al., EEG-Linked functional magnetic resonance imaging in epilepsy and cognitive neurophysiology, in J Clin Neurophysiol. 2000. p. 43--58.
10. Briselli, E., et al., An independent component analysis-based approach on ballistocardiogram artifact removing, in Magnetic Resonance Imaging. 2006. p. 393--400.
11. Nakamura, W., et al., Removal of ballistocardiogram artifacts from simultaneously recorded EEG and fMRI data using independent component analysis, in IEEE Trans Biomed Eng. 2006. p. 1294--1308.
12. Haag, A., et al., Emotion Recognition Using Bio-sensors: First Steps towards an Automatic System, in international Tutorial and Research Workshop on Affective Dialogue Systems,Germany. 2004. p. 36-48.

Author: Jacek Lukasz Kustra
Institute: IEETA – University of Aveiro
Street: Campus Univ. de Santiago
City: Aveiro
Country: Portugal
Email: jacek@ua.pt

References

[1] V. X. Afonso, W. J. Tompkins, T. Q. Nguyen, and Shen Luo. Ecg beat detection using filter banks. *Biomedical Engineering, IEEE Transactions on*, 46(2):192–202, 1999.

[2] Philip J. Allen, Giovanni Polizzi, Karsten Krakow, David R. Fish, and Louis Lemieux. Identification of eeg events in the mr scanner: The problem of pulse artifact and a method for its subtraction. *NeuroImage*, 8(3):229–239, October 1998.

[3] S. Amari and A. Cichocki. Adaptive blind signal processing-neural network approaches. *Proceedings of the IEEE*, 86(10):2026–2048, 1998.

[4] Kimitaka Anami, Takeyuki Mori, Fumiko Tanaka, Yusuke Kawagoe, Jun Okamoto, Masaru Yarita, Takashi Ohnishi, Masato Yumoto, Hiroshi Matsuda, and Osamu Saitoh. Stepping stone sampling for retrieving artifact-free electroencephalogram during functional magnetic resonance imaging. *Neuroimage*, 19(2 Pt 1):281–295, Jun 2003.

[5] Richard Bellman. *Dynamic Programming*. Princeton Univ Pr, 1957.

[6] Christian-G. Benar, Yahya Aghakhani, Yunhua Wang, Aaron Izenberg, Abdullah Al-Asmi, Francois Dubeau, and Jean Gotman. Quality of eeg in simultaneous eeg-fmri for epilepsy. *Clinical Neurophysiology*, 114(3):569–580, March 2003.

[7] Giorgio Bonmassar, Patrick L Purdon, Iiro P Jskelinen, Keith Chiappa, Victor Solo, Emery N Brown, and John W Belliveau. Motion and ballistocardiogram artifact removal for interleaved recording of eeg and eps during mri. *Neuroimage*, 16(4):1127–1141, Aug 2002.

[8] Ennio Briselli, Girolamo Garreffa, Luigi Bianchi, Marta Bianciardi, Emiliano Macaluso, Manuel Abbafati, Maria Grazia Marciani, and Bruno Maraviglia. An independent component analysis-based approach on ballistocardiogram artifact removing. *Magnetic Resonance Imaging*, 24(4):393–400, May 2006.

[9] J. D. Bronzino. *The Biomedical Engineering Handbook*. CRC, 1995.

[10] Zhiyi Chi, Wei Wu, Zach Haga, Nicholas G Hatsopoulos, and Daniel Margoliash. Template-based spike pattern identification with linear convolution and dynamic time warping. *J Neurophysiol*, 97(2):1221–1235, Feb 2007.

[11] A. Cichocki. Icalab. `www.bsp.brain.riken.jp/ICALAB/`.

[12] Stuart Clare. *Functional MRI : Methods and Applications*. PhD thesis, University of Nottingham, 1997.

[13] M. S. Cohen and R. M. DuBois. Stability, repeatability, and the expression of signal magnitude in functional magnetic resonance imaging. *Journal of Magnetic Resonance Imaging*, 10(1):33–40, July 1999.

[14] Pierre Comon. Independent component analysis, a new concept? *Signal Process.*, 36(3):287–314, 1994.

[15] A. Delorme and S. Makeig. Eeglab: an open source toolbox for analysis of single-trial eeg dynamics including independent component analysis. *Journal of Neuroscience Methods 134*, pages 9–21, 2004.

[16] Jose Maria Fernandes. *piGauss: spatio-temporal characterization of brain activity in Epilepsy*. PhD thesis, Universidade de Aveiro, 2007.

[17] C Fonseca, J. P. S Cunha, R. E. Martins, V. Ferreira, J. P. Marques de S, M. A. Barbosa, and A. Martins da Silva. A novel dry active electrode for eeg recording. *IEEE Transactions on Biomedical Engineering*, 54:162–165, 2007.

[18] G. Garreffa, M. Carni, G. Gualniera, G. B. Ricci, L. Bozzao, D. De Carli, P. Morasso, P. Pantano, C. Colonnese, V. Roma, and B Maraviglia. Real-time mr artifacts filtering during continuous eeg/fmri acquisition. *Magnetic Resonance Imaging*, 21(10):1175–1189, December 2003.

[19] R. I. Goldman, J. M. Stern, J. Engel, and M. S. Cohen. Acquiring simultaneous EEG and functional MRI. *Clinical Neurophysiology*, 111(11):1974–1980, November 2000.

[20] A. Haag, S. Goronzy, P. Schaich, and J. Williams. Emotion recognition using bio-sensors: First steps towards an automatic system. *international Tutorial and Research Workshop on Affective Dialogue Systems,Germany*, pages 36–48, 2004.

[21] R. A. Hill, K. H. Chiappa, F. Huang-Hellinger, and B. G. Jenkins. Hemodynamic and metabolic aspects of photosensitive epilepsy revealed by functional magnetic resonance imaging and magnetic resonance spectroscopy. *Epilepsia*, 40(7):912–920, Jul 1999.

[22] A. Hoffmann, L. Jger, K.J. Werhahn, M. Jaschke, S. Noachtar, and M. Reiser. Electroencephalography during functional echo-planar imaging: Detection of epileptic spikes using post-processing methods. *Magnetic Resonance in Medicine*, 44(5):791–798, 2000.

[23] H. C. Huang and B. H. Jansen. Eeg waveform analysis by means of dynamic time-warping. *Int J Biomed Comput*, 17(2):135–144, Sep 1985.

[24] H.H. Jasper. The ten-twenty electrode system of the international federation. *Electroencephalogram and Clinical Neurophysiology*, 10:371–375, 1958.

[25] V Jurcal, D Tsuzuki, and I Dan. 10/20, 10/10, and 10/5 systems revisited: Their validity as relative head-surface-based positioning systems. *Neuroimage*, 34:1600–1611, 2007.

[26] E. Keogh and M. Pazzani. Derivative dynamic time warping, 2001.

[27] Kyung Hwan Kim, Hyo Woon Yoon, and Hyun Wook Park. Improved ballistocardiac artifact removal from the electroencephalogram recorded in fmri. *Journal of Neuroscience Methods*, 135(1-2):193–203, May 2004.

[28] B. U. Kohler, C. Hennig, and R. Orglmeister. The principles of software qrs detection. *Engineering in Medicine and Biology Magazine, IEEE*, 21(1):42–57, 2002.

[29] K. Krakow, P. J. Allen, M. R. Symms, L. Lemieux, O. Josephs, and D. R. Fish. Eeg recording during fmri experiments: image quality. *Hum Brain Mapp*, 10(1):10–15, May 2000.

[30] Einat Liebenthal, Michael L Ellingson, Marianna V Spanaki, Thomas E Prieto, Kristina M Ropella, and Jeffrey R Binder. Simultaneous erp and fmri of the auditory cortex in a passive oddball paradigm. *Neuroimage*, 19(4):1395–1404, Aug 2003.

[31] Frank Masterpasqua and Kathryn December 2003 Healey. Neurofeedback in psychological practice. *Professional Psychology: Research and Practice*, 34:652–656, 2003.

[32] T. Matsushima, Y. Morikiyo, and Y. Fujishima. [analysis of handwriting by the dynamic programming matching]. *Shinrigaku Kenkyu*, 64(5):351–359, Dec 1993.

[33] C Michel, Micah M Murray, Goran Lantz, S Gonzalez, Andino, L Spinelli, and 2004. Grave de Peralta Menendez, R 115: 2195-2222. Eeg source imaging. *Clinical Neuphysiology*, 115:2195–2222, 2004.

[34] R. M. Mri, J. Felblinger, K. M. Rsler, B. Jung, C. W. Hess, and C. Boesch. Recording of electrical brain activity in a magnetic resonance environment: distorting effects of the static magnetic field. *Magn Reson Med*, 39(1):18–22, Jan 1998.

[35] W. Nakamura, K. Anami, T. Mori, O. Saitoh, A. Cichocki, and S. Amari. Removal of ballistocardiogram artifacts from simultaneously recorded eeg and fmri data using independent component analysis. In *IEEE Trans Biomed Eng* [35], pages 1294–1308.

[36] R. Niazy. The fmrib plug-in for eeglab.

[37] S. Oswaga, T. M. Lee, A. R. Kay, and D. W. Tank. Brain magnetic resonance imaging with contrast dependent on blood oxygenation. *Proceedings of the National Academy of Sciences*, 89:9868–9872, 1990.

[38] J. Arthurs Owen and Simon Boniface. How well do we understand the neural origins of the fmri bold signal? *Trends in Neurosciences*, 25:27–31, 2002.

[39] J. Pan and W. J. Tompkins. A real-time qrs detection algorithm. *IEEE Trans Biomed Eng*, 32(3):230–236, March 1985.

[40] Y. Qi. Time normalization in voice analysis. *J Acoust Soc Am*, 92(5):2569–2576, Nov 1992.

[41] J Rowan and A Tolunsky. *Primer of EEG*. Butterworth-Heinemann, 2003.

[42] Carl Sagan. *The Dragons of Eden: Speculations on the Evolution of Human Intelligence*. Ballantine Books, 1978.

[43] Afraim Salek-Haddadi, Louis Lemieux, Martin Merschhemke, Beate Diehl, Philip J Allen, and David R Fish. Eeg quality during simultaneous functional mri of interictal epileptiform discharges. *Magnetic Resonance Imaging*, 21(10):1159–1166, December 2003.

[44] D. L. Schomer, G. Bonmassar, F. Lazeyras, M. Seeck, A. Blum, K. Anami, D. Schwartz, J. W. Belliveau, and J. Ives. Eeg-linked functional magnetic resonance imaging in epilepsy and cognitive neurophysiology. *J Clin Neurophysiol*, 17(1):43–58, Jan 2000.

[45] M. S Schwartz and F. Andrasik. *Biofeedback: A Practitioner's Guide*. The Guilford Press; 3 edition, 2003.

[46] M. Seeck, F. Lazeyras, C. M. Michel, O. Blanke, C. A. Gericke, J. Ives, J. Delavelle, X. Golay, C. A. Haenggeli, N. de Tribolet, and T. Landis. Non-invasive epileptic focus localization using eeg-triggered functional mri and electromagnetic tomography. *Electroencephalogr Clin Neurophysiol*, 106(6):508–512, Jun 1998.

[47] R. B. Selim. Eeg atlas: Eeg artifacts. http://www.emedicine.com/neuro/topic678.htm, September 2006.

[48] J. Sijbers, J. Van Audekerke, M. Verhoye, A. Van der Linden, and D. Van Dyck. Reduction of ecg and gradient related artifacts in simultaneously recorded human eeg/mri data. *Magnetic Resonance Imaging*, 18(7):881–886, September 2000.

[49] G. Srivastava, S. Crottaz-Herbette, K.M. Lau, G.H. Glover, and V. Menon. Ica-based procedures for removing ballistocardiogram artifacts from eeg data acquired in the mri scanner. *NeuroImage*, 24(1):50–60, January 2005.

[50] Xiaohong Wan, Kazuki Iwata, Jorge Riera, Masaharu Kitamura, and Ryuta Kawashima. Artifact reduction for simultaneous eeg/fmri recording: Adaptive fir reduction of imaging artifacts. *Clinical Neurophysiology*, 117(3):681–692, March 2006.

[51] K. Wang, H. Begleiter, and B. Porjesz. Warp-averaging event-related potentials. *Clin Neurophysiol*, 112(10):1917–1924, Oct 2001.

[52] S. Warach, J. R. Ives, G. Schlaug, M. R. Patel, D. G. Darby, V. Thangaraj, R. R. Edelman, and D. L. Schomer. Eeg-triggered echo-planar functional mri in epilepsy. *Neurology*, 47(1):89–93, Jul 1996.

[53] M Woods and M. B. Woods. *The history of Medicine*. Twenty-First Century Books, 2005.